Cyclin-dependent kinase 5 (Cdk5) activity is modulated by light and gates rapid phase shifts of the circadian clock

Andrea Brenna[1,2,*], Micaela Borsa[3,4], Gabriella Saro[1] , Jürgen A. Ripperger[1], Dominique A. Glauser[1], Zhihong Yang[2], Antoine Adamantidis[3,4] & Urs Albrecht[1,*]

[1] Department of Biology, University of Fribourg, Fribourg, Switzerland
[2] Department of Medicine, University of Fribourg, Fribourg, Switzerland
[3] Zentrum für Experimentelle Neurologie, Department of Neurology, Inselspital, Bern University Hospital, University of Bern, Bern, Switzerland
[4] Department of Biomedical Research, University of Bern, Bern, Switzerland

*corresponding authors: andrea.brenna@unifr.ch, urs.albrecht@unifr.ch

Abstract

The circadian clock allows organisms to coordinate biochemical and physiological processes over one day. Changes in lighting conditions as they occur naturally over seasons or manmade by jet lag or shift work, advance or delay clock phase to synchronize physiology to the environment. Within the suprachiasmatic nucleus (SCN) of the hypothalamus, circadian timekeeping and resetting have been shown to depend on both membrane depolarization and intracellular second-messenger signaling. In both processes, voltage-gated calcium channels (VGCCs) mediate calcium influx resulting in the activation of intracellular signaling pathways that activate *Period* (*Per*) gene expression. However, the precise mechanism how these processes are gated in a concerted manner is unknown. Here we show that cycling-dependent kinase 5 (Cdk5) activity is modulated by light and gates phase shifts of the circadian clock. We found that knock-down of *Cdk5* in the SCN of mice affects phase delays but not phase advances. This is associated with uncontrolled calcium influx into SCN neurons and an unregulated protein kinase A (PKA) – calcium calmodulin dependent kinase (CaMK) – cAMP response element-binding protein (CREB) signaling pathway. Accordingly, genes such as *Per1* are not induced by light in the SCN of *Cdk5* knock-down mice. Our experiments identified an important light modulated kinase that affects rapid clock phase adaptation. This finding indicates how light responsiveness and clock phase are coordinated to adapt activity onset to seasonal changes, jet-lag and shift work.

The circadian system coordinates biochemical and physiological functions in our body and synchronizes them to the environmental day-night cycle. Misalignment of the internal body clock with the external light-dark cycle, induced by shift work or jet lag, leads to inefficient regulation of body functions. As a consequence, circadian misalignment can lead to obesity, cancer, addictive behaviors, cardiovascular disease, and neurological disorders [1]. Therefore, it is crucial to understand how the environment impacts the clock and how these entities interact.

In mammals, the master circadian clock is located in the ventral part of the hypothalamus just above the optic chiasm in the suprachiasmatic nuclei (SCN), which coordinate daily cycles of physiology and behavior [2]. Molecular daily oscillations are generated at the cellular level by a cell-autonomous transcription-translation feedback loop (TTFL) involving a set of clock genes [3] and post-translational modifiers such as kinases [4, 5]. Circuit-level interactions among SCN cells produce a coherent daily oscillation [6], which can be modulated by light signals to match the environmental light-dark cycle. Light is perceived by melanopsin containing photosensitive retinal ganglion cells (pRGCs) in the eye, and the signal produced in these cells travels via the retinohypothalamic tract (RHT) to the SCN [7]. The release of glutamate at the RHT terminals stimulates AMPA/NMDA receptors, leading to Ca^{2+} influx into the SCN [8]. Additionally, the activity of various kinases is changed, including DARPP-32 (dopamine and cAMP-regulated phosphoprotein of 32 kD), PKA (protein kinase A), and CaMK (Ca^{2+}/calmodulin-dependent kinases). This cascade finally culminates in the phosphorylation of CREB (cyclic AMP response element binding protein) [9, 10, 11, 12, 13]. This event promotes chromatin phosphorylation [14] and acetylation via the recruitment of CRTC1 (cAMP-regulated transcriptional co-activator 1) and the histone acetyltransferase CBP (CREB-binding protein), involving the clock protein PER2 [15]. As a consequence, immediate-early gene and clock gene expression is induced [16, 17, 18], causing a phase shift of the TTFL in oscillating cells of the SCN [6]. This manifests at the behavioral level in a change of locomotor activity onset (phase shift) the day after the light pulse. The direction of the phase shift depends on the clock's temporal state. Light perceived in the early night promotes phase delays. On the other hand, a light pulse late at night promotes phase advances, whereas light in the middle of the day does not alter the clock phase [19]. For this so-called resetting of the circadian clock, the *Per1* and *Per2* genes appear to be important in the mouse. While *Per1* is essential for phase advances, *Per2* function is necessary for phase delays [20, 21].

Voltage-gated calcium channels (VGCCs) are classified into high voltage-activated channels (HVA), which include L-type and low voltage-activated (LVA) subtypes, also known as T-type channels [22]. T-type VGCCs are involved in phase delays, whereas L-type VGCCs are related to phase advances [23, 24]. $Ca_V3.1$, $Ca_V3.2$, and $Ca_V3.3$ belong to the T-type channel family, which is critically important for neuronal excitability [25]. The activity of these T-type channels are regulated by various kinases, including PKA [26], PKC [27], and CDK5 (cyclin-dependent kinase 5) [28].

Cdk5 is a proline-directed serine/threonine kinase that forms a complex with its neural activators p35 or p39 [29, 30] and cyclin I [31]. The complex of Cdk5 and its activators controls various neuronal processes such as neurogenesis, neuronal migration, and synaptogenesis [32, 33]. *In vivo* and *in vitro* experiments show that Cdk5 kinase activity is low in the light phase and high in the dark phase [34, 35]. It regulates the circadian clock in the SCN via phosphorylation of PER2 at serine 394 ($Per2^{Brdm}$ domain). Upon phosphorylation by Cdk5, PER2 is stabilized and enters the nucleus to participate in the regulation of the TTFL and CREB-related transcriptional events [15, 34]. Since Cdk5 regulates the T-type channel $Ca_V3.1$ [28] and the circadian clock via PER2 phosphorylation [34], we analyzed a potential role of Cdk5 in the light-mediated clock resetting mechanism.

Results

Cdk5 knock-down in the SCN impairs light-induced phase delays. Light perceived in the dark period elicits changes in the clock phase [19]. To test whether *Cdk5* plays a role in this process, we knocked down *Cdk5* in the SCN via stereotaxic application of adeno-associated viruses (AAVs). We injected an adenovirus expressing shRNA to silence *Cdk5* (shCdk5) and, as a control, an adenovirus expressing a control shRNA (scr) into the SCN [34]. Consistent with our previous observations [34], we found that silencing *Cdk5* in the SCN reduced its expression in the SCN (Supplementary Fig. 1a) and the expression of PER2 (Supplementary Fig. 1b). Under constant darkness (DD) conditions this knock-down of *Cdk5* shortened clock period in mice as assessed by wheel-running activity (Fig. 1a, b and Supplementary Fig. 1c). This period was not influenced by light pulses (Supplementary Fig. 1d). However, onset of activity was affected after releasing mice into constant darkness (DD). Light at zeitgeber time (ZT) 14 (where ZT0 is lights on and ZT12 is lights off) delayed the clock phase, whereas light at ZT22 advanced it in control (scr) animals, with light at ZT10 having no effect (Fig. 1a, c, Aschoff type II protocol). The animals with silenced *Cdk5* in the SCN (shCdk5) behaved similarly to controls (scr), except for ZT14. Light did not elicit a phase delay at this time, suggesting that *Cdk5* plays a role in the phase delay mechanism.

To corroborate our observations, we performed the same experiment in DD (Aschoff type I protocol). The shCdk5 animals displayed a shorter period compared to scr controls (Fig. 1d, e), consistent with previous observations [34]. After determination of each animal's clock period, we administered light pulses of 15 min. at circadian times (CT) 10, CT14, and CT22 for each animal (orange stars, Fig. 1d). Light at CT10 had no effect on both the shCdk5 and scr control mice (Fig. 1f). Light applied at CT14 promoted a phase delay in scr control mice. However, silencing of *Cdk5* impaired the delay of the clock phase (Fig. 1d, f), which is consistent with the observation at ZT14 (Fig. 1a, c). Light at CT22 elicited normal phase advances in shCdk5 and scr controls (Fig. 1d, f), similar to the light pulse applied at ZT22 (Fig. 1a, c). From these experiments, we conclude that *Cdk5* plays a role in delaying the clock phase in response to a light pulse in the early activity period of mice.

Cdk5 activity is modulated by light in the early night. Since we observed that Cdk5 plays a significant role in the phase shift of the circadian clock, we questioned whether the light signal at ZT14 could affect the levels of Cdk5 and its co-activator p35 in the SCN. To this end, we collected SCN samples at ZT14 in the dark or after a 15 min. light pulse, and we performed a western blot on total protein extracts. To control proper light induction, we measured the light-dependent phosphorylation of PKA (Fig. 2a, b) and CaMKII (Supplementary Fig. 2a, b). We confirmed that PKA and CaMKII phosphorylation levels were increased by light in the SCN (Fig. 2a, b, Supplementary Fig. 2a, b). Interestingly, we observed that light could also increase the p35 protein level, although the levels of Cdk5 were not affected (Fig. 2a, c). Because the levels of the Cdk5 co-activator p35 were increased by light, we wondered whether this event would affect the kinase activity of Cdk5/p35. We performed an *in vitro* kinase assay using the immunoprecipitated Cdk5 present in SCN tissue collected from mice not exposed to light or exposed to light at ZT14. We used the recombinant histone H1 as substrate in the presence of radioactive ATP [34]. Surprisingly, our results indicated that Cdk5 kinase activity was decreased by light (Fig. 2d, e), suggesting that light may affect the interaction between Cdk5 and p35. Therefore, we performed a co-immunoprecipitation experiment using an antibody against Cdk5 as bait to challenge this hypothesis. Our results revealed that the SCN extract from mice that received a light pulse at ZT14 contained less pulled down p35 in a complex with Cdk5 (Fig. 2f). Taken together, the results support the hypothesis that light affects Cdk5 activity via interference with the

formation of a complex of Cdk5 with its co-activator p35. Interestingly, the light pulse at ZT14 might affect more than just Cdk5/p35 protein: protein interactions and additional unknown proteins may be involved (Supplementary Fig. 2c).

Cdk5 impacts the CREB signaling pathway via calcium/calmodulin-dependent kinases (CaMK). Deletion of a cAMP-responsive element (CRE) in the *Per1* promoter blunted light-induced *Per1* expression in the SCN at night [36]. Because nocturnal light induces phosphorylation of CRE binding protein (CREB) and phosphorylated CREB (p-CREB) can bind to CREs [37, 38, 39], we investigated whether Cdk5 is involved in the pathway evoking the CREB phosphorylation at serine-133 (pSer-133), a site known to be involved in phase delays, and *Per1* induction [11]. Therefore, we performed immunohistochemical analysis using an antibody detecting phosphate on CREB at serine 133 (p-CREB-S133) (Fig. 3a, Supplementary Fig. 3b, control Supplementary Fig. 3c). In the SCN of control animals (scr), we observed p-CREB-S133 in nuclei of neurons after the light was delivered at ZT14 but not in controls (Fig. 3a, arrowheads). In contrast, p-CREB-S133 was already detected in nuclei before the light pulse in shCdk5 animals (Fig. 3a, arrowheads), indicating that *Cdk5* plays a role in gaiting the phosphorylation of CREB.

The CREB/CRE transcriptional pathway has been shown to be activated by calcium/calmodulin-dependent kinase II (CaMKII) and mitogen-activated protein kinase (MAPK) [40, 41, 42]. Pharmacological inhibition of CaMKII but not of MAPK affected light-induced phase delays in hamsters [43]. Therefore, we tested whether phosphorylated CaMKII (p-CaMKII) is affected by the knock-down of *Cdk5* in the SCN of mice. We observed that p-CaMKII presence (alpha isoform) in the cytoplasm of SCN cells increased after light at ZT14 compared to no light in control animals (Fig. 3b, left panels). In shCdk5 SCN, however, p-CaMKII was already present before the light pulse in significantly higher levels than controls (Fig. 3b, control Supplementary Fig. 3d). This result indicates that *Cdk5* is gating the phosphorylation of CaMKII alpha.

CaMKII has been shown to shuttle Ca^{2+}/calmodulin (Ca^{2+}/CAM) to the nucleus to trigger CREB phosphorylation and gene expression [44]. Therefore, we investigated whether CAM localization was influenced by a light pulse and whether *Cdk5* plays a role in this process. We observed that in control animals, CAM was distributed evenly in the cytoplasm of cells in SCN tissue before a light pulse. However, after the light pulse, it was localized around the nuclei (Fig. 3c). Interestingly, in the SCN of shCdk5 animals, CAM was already localized around the nuclei before the light administration and remained there after the light pulse, suggesting that *Cdk5* is gating CAM localization in the cell.

Once delivered to the nucleus, Ca^{2+}/CAM triggers a highly cooperative activation of the nuclear CaMK cascade, including CaMKIV, to rapidly phosphorylate CREB for the transcription of target genes [44, 45]. Therefore, we tested whether a light pulse affected the phosphorylation of CaMKIV and whether this was influenced by *Cdk5*. In control animals, we detected p-CaMKIV to be strongly present in the SCN after but not before a light pulse (Fig. 3d, control Supplementary Fig. 3e). In shCdk5 SCN, p-CaMKIV was always detectable independent of the light pulse (Fig. 3d). This indicated that Cdk5 was gating phosphorylation of CaMKIV.

Calcium entry is regulated by channels, such as T-type VGCC, which are involved in phase delays [23]. Previous reports show that Cdk5 directly or indirectly can phosphorylate Cav3.1 *in vitro* [28]. Thus, we looked at the influence of light and *Cdk5* on the T-type channel Cav3.1 using immunohistochemical staining. We observed that the level of Cav3.1 protein was significantly increased on the surface of SCN cells after the light pulse (Fig. 3e, blue bars). This suggests that light inhibits internalization and degradation of this channel. Interestingly, in the *Cdk5* depleted SCN cells, Cav3.1 staining was already high on the cell

surface before the light signal (Fig. 3e, red bars). We observed no difference in the Cav3.1 signal between SCN samples obtained from shCdk5 mice before and after the light pulse (Fig. 3e, red bars), suggesting that *Cdk5* may be directly or indirectly involved in the regulation of Cav3.1 localization. This is consistent with previously described effects of Cdk5 on the cellular localization of other receptors such as the D2 and TRPV1 receptors [46, 47].

Cdk5 modulates neuronal activity in response to light at ZT14. Neuronal activity in response to light at ZT14 requires calcium influx. At night neuronal cell membranes are hyperpolarized, creating a Ca^{2+} gradient. A light stimulus at night promotes membrane depolarization and VGCC activation, which evokes a Ca^{2+} influx into SCN neurons ultimately changing the phase of the circadian clock [48, 49]. Our results shown in figure 3 indicate that Cdk5 regulates the gating between light and the CaMKII pathway, which relies on Ca^{2+} availability. Thus, we tested whether Cdk5 regulated the light-mediated Ca^{2+} influx into SCN neurons. To this end, we employed *in vivo* calcium imaging to assess changes in calcium levels in the SCN in freely moving mice after 15 minutes of a light pulse given at ZT14. First, we injected an adeno-associated virus (AAV) expressing the shCdk5 sequence into the SCN to silence *Cdk5*. This AAV is co-expressing the calcium indicator GCaMP7 under the neuron-specific synapsin 1 promoter. As a control, we injected an AAV carrying a NSshRNA (scrambled sequence) instead of shCdk5 (see Materials and Methods). Consistent with our previous results, the construct expressing shCdk5 in the SCN produced a shortened free-running period in mice (Supplementary Fig. 4a-c). Animals injected with AAV were implanted with a chronic optical fiber placed above the SCN to allow for longitudinal imaging of GCaMP7 signals using fiber photometry. After habituation, $\Delta F/F_0$ (or the ratio of change in GCaMP7 fluorescence to the baseline fluorescence, see methods) was recorded before and after light pulse delivery at ZT14 in both groups of mice (Fig. 4a).

We observed an increase of calcium activity in control mice (scramble) during 15 min. of the light pulse at ZT14, which was also sustained for over 15 min. after the light pulse (Fig. 4b, black trace). In contrast, the $\Delta F/F_0$ in shCdk5 mice during and after the 15 min. light pulse was significantly lower compared to the control animals (Fig. 4b, red trace). Interestingly, we could observe random, but regular calcium transients, unrelated to the light stimulus during and after the light pulse (Fig. 4b, at -1, 2-3, 9, 12, and 14 min during the light pulse and 5, 9 and 12 min after the light pulse). A Ca^{2+} transient was observed right before the light was given at ZT14 (Fig. 4b), which showed the same magnitude as those observed during and after the light stimulus.

This activity was significantly decreased in shCdk5 mice during the last five minutes of the light pulse as compared to the baseline levels (see Methods; Fig. 4c; Supplementary Fig. 4d). Interestingly, 5 min. and 15 min. after the light pulse, the calcium mediated activity remained significantly lower in shCdk5 animals compared to controls (Fig. 4c and Supplementary Fig. 4d). Finally, mice were sacrificed, and the GFP signal was assessed by immunostaining to verify virus expression in the SCN (Fig. 4d). The outlined circle in red indicates where the fibers were located. Taken together, these results indicate that Cdk5 modulates Ca^{2+} mediated neuronal signaling.

Cdk5 regulates the DARPP32-PKA axis. The cAMP-activated Protein Kinase A (PKA) signaling pathway, leading to phosphorylation of CREB, plays a pivotal role in regulating phase delays in photic resetting [50, 51]. Since the PKA signaling pathway can be induced in vivo [10, 52] and in vitro [53], we wondered whether Cdk5 could play a role in PKA- mediated CREB phosphorylation. To this end, we employed Förster resonance energy transfer (FRET) a widely used method to investigate molecular interactions between proteins such as CREB: CBP in living cells [15, 54].

We transfected control (wt) and *Cdk5* knock-out (*Cdk5* KO) NIH 3T3 cell lines [34] with ICAP (an indicator of CREB activation due to phosphorylation) and stimulated the cells with forskolin in presence of Ca^{2+}. Phosphorylation of the CREB domain in the reporter decreased the FRET signal after 30 min. while non phosphorylation increased it. We observed that the FRET signal in wt cells strongly decreased within 30 min. after the stimulus compared to baseline (Fig. 5a, blue trace). In contrast, the FRET signal in *Cdk5* KO cells rose towards baseline after an initial decline in response to forskolin (Fig. 5a, red trace). This indicated that Cdk5 is involved in the phosphorylation of CREB. Of note is that the forskolin solvent DMSO can't stimulate CREB phosphorylation on its own (Supplementary Fig. 5a).

Previous studies have described that Ca^{2+}-mediated CREB transcription of target genes requires PKA activity [42]. However, to date it is not clear whether there is a parallel (synergistic) relationship between PKA and Ca^{2+} signaling pathways or whether they are sequentially depending on each other (Fig 5b, cartoon model). To address this question, we performed the following FRET experiment. NIH 3T3 cells were stimulated with forskolin in either the presence of Ca^{2+} with EGTA (Ca^{2+} chelator) (Fig. 5b, orange line), without EGTA (Fig. 5b, blue line) or completely depleted of Ca^{2+} (Fig. 5b, salmon colored line). We observed that under normal conditions the FRET signal goes down, comparable to the signal seen in figure 5a, indicating a higher Ser-133 KID phosphorylation compared to the baseline (Fig 5b, blue signal). When we added EGTA (removing Ca^{2+}), the FRET signal increased to the baseline level after the forskolin treatment (Fig 5b, orange signal). The cells depleted of Ca^{2+} were also not responsive to the forskolin stimulus since the FRET signal moved towards the baseline level within 30 min. (Fig. 5b, salmon colored signal). Together, our results indicate that CREB phosphorylation is modulated by Cdk5 via Ca^{2+} signaling as suggested in figure 3. Interestingly, PKA appeared not to directly phosphorylate CREB, because CREB did not pull-down p-PKA in an immunoprecipitation experiment. In contrast p-CaMKIV did interact with CREB (Supplementary Fig. 5b, c) suggesting that CREB is most likely phosphorylated by CaMKIV, which is probably indirectly regulated by PKA activity.

Next, we aimed to investigate what the possible pathway could be through which PKA regulates CaMKIV. Previous studies have shown that Cdk5 regulates PKA activity via DARPP32 [55] (Fig. 5c). Therefore, we asked whether DARPP32 phosphorylation was light-dependent and whether Cdk5 would modulate this process. We sacrificed mice either receiving a light pulse at ZT14 or no light. Cryo-sections containing the SCN were stained with an antibody recognizing phosphorylated Thr-75 (pThr-75) of DARPP32. We observed that DARPP32 is highly phosphorylated at ZT14 with the light signal reducing the phosphorylation levels in the cytoplasm and nuclei significantly (Fig. 5d, blue bars; Supplementary Fig. 5d, e). In contrast, silencing of *Cdk5* led to a dramatic decrease of the pThr-75 signal in the cytoplasm and nuclei of SCN cells at ZT14 and light did not have an effect (Fig. 5d, red bars, Supplementary Fig. 5e). These observations are consistent with the view that Cdk5 phosphorylates DARPP32 and that light inhibits this process probably through an unknown mechanism inactivating Cdk5.

Non phosphorylated DARPP32 promotes PKA activity, which is characterized by phosphorylation at Thr-197 in the catalytic site of PKA [56, 57]. Therefore, we asked whether decreased levels of p-DARPP32 after the light stimulus at ZT14 could inversely correlate with the phosphorylation state of PKA. Thus, we performed immunostaining on coronal brain sections containing the SCN using an antibody recognizing the phosphorylated Thr-197 of PKA. We observed that PKA phosphorylation significantly increased after the light pulse in the SCN tissue obtained from control (scr) mice (Fig. 5e, right panel, blue bars). However, in SCN from shCdk5 mice, the phosphorylation level was already elevated before the light pulse compared to scr control (Fig. 5e, left panels, top micrographs), and it was also sustained after the light pulse (Fig. 5e, left panels, bottom micrographs, right panel, red bars). Our results

indicate that Cdk5 gates PKA phosphorylation induced by the light pulse at ZT14. Many observations indicate that active PKA can stimulate the Ca^{2+} influx through Cav3 T-type voltage gated channels, including Cav3.1 [27, 58]. The molecular mechanism normally requires physical interaction between the channel and PKA, followed by phosphorylation which influences the gating properties [59]. Therefore, we performed a co-immunostaining in the same SCN sections collected before (Fig. 3) to detect both Cav3.1 and phospho-PKA (the active form). We observed that the colocalization between Cav3.1 and phospho-PKA dramatically increased after the light pulse in the SCN tissue of control (scr) mice (Fig. 5f, scr left panels yellow color, and blue bars in the right panel). Interestingly, the colocalization level of the two proteins was already high in the shCdk5 SCN tissue before the light pulse, compared to controls (Fig. 5f scramble vs. shCdk5, left panel, top micrographs). The colocalization level between Cav3.1 and phospho-PKA in the shCdk5 tissues was not influenced by the light pulse (Fig. 5f, right panel, red bars). Altogether our results suggest that Cdk5 gates the PKA-Cav3.1 interaction in response to the light signal at ZT14 in an indirect way via DARPP32.

Cdk5 affects light-induced gene expression. Light perceived in the dark period leads not only to phase shifts but is also paralleled by the induction of immediate early genes and certain clock genes in the SCN [16, 17, 18, 60, 61]. This process involves the PKA – CaMK – CREB signaling pathway (reviewed in [62]). Therefore, we investigated whether Cdk5 is involved in the signal transduction process to induce immediate early genes and clock genes in the SCN in response to light. To that extent, we performed a time-course profile of light-induced genes and immediate early genes. We collected SCN from mice that received a nocturnal light pulse at ZT14 at different time points after the stimulus over 2 hours (Fig. 6). In agreement with previous studies, *Per1* and *Dec1* mRNA expression was induced by light peaking at 1h after the stimulus. Conversely, *Per2* and *Dec2* mRNA expression was not affected by the light pulse at ZT14 (Fig. 6a-d, blue bars) [18, 61, 63]. Knock-down of *Cdk5* abolished this light-driven *Per1* and *Dec1* gene induction (Fig. 6a, c, red bars), indicating an involvement of *Cdk5* in the light-driven activation process of these clock genes. As previously reported, expression of the clock gene *Bmal1* was not light-inducible [34, 64] and not affected by shCdk5 (Fig. 6e). The injection of the control scr and shCdk5 constructs was successful, as demonstrated by the expression of *eGFP* mRNA in the analyzed SCN (Fig. 6f).

Interestingly, the knock-down of *Cdk5* did not affect light-mediated induction of *cFos* expression, which peaked at 0.5h after the light pulse (Fig. 6g). In contrast, *Egr1*, another immediate early gene, which is involved in synaptic plasticity, learning, and memory [65], was light-inducible in control but not in shCdk5 animals (Fig. 6h). This suggests that the immediate early gene *cFos* is regulated by a different mechanism compared to *Egr1* and the clock genes *Per1* and *Dec1* in response to a light stimulus at ZT14.

Vasoactive intestinal polypeptide (VIP) was described to play a role in phase-shifting the SCN clock [66]. Furthermore, the light-induced expression of clock genes is localized in VIP-positive cells in the SCN that are essential for clock resetting [67]. Therefore, we tested whether *Vip* gene expression is affected by shCdk5. We observed that a light pulse did not induce *Vip* expression significantly in the SCN, nor did shCdk5 affect its general expression (Supplementary Fig. 6a). This suggests that *Cdk5* does not regulate *Vip* expression and modulate phase shifts via VIP.

Salt inducible kinase 1 (*Sik1*) is involved in the regulation of the magnitude and duration of phase shifts by acting as a suppressor of the effects of light on the clock [68]. Therefore, we tested how a light pulse affected *Sik1* expression in the SCN and whether *Cdk5* might play a role in its regulation. We observed that *Sik1* was significantly induced by a light pulse in the SCN of control mice after 0.5 h. However, the knock-down of *Cdk5* abolished this induction

(Fig. 6i). This suggests that *Cdk5* modulates *Sik1* expression to regulate the magnitude of the behavioral response to light.

The light-inducible small G-protein Gem limits the circadian clock phase-shift magnitude by inhibiting voltage-dependent calcium channels [69]. We tested whether a light pulse affected *Gem* expression in the SCN and whether this was involving Cdk5. We observed that Gem was significantly induced by light 1 hour after light administration (Fig. 6j, blue bars). Interestingly, knock-down of *Cdk5* abolished this induction (Fig. 6i, red bars), but *Gem* levels seemed to be slightly but not significantly elevated already before light administration (Fig. 6i, time point 0). This indicates that Cdk5 influences light induced *Gem* expression and that Cdk5 may also affect basal *Gem* expression before the light pulse. Interestingly, similar results as for light induced gene expression in shCdk5 SCN were observed in SCN of *Per2*^{Brdm1} mutant mice (Supplementary Fig. 6b, c).

Phase shifts of the circadian clock can also be studied in cell cultures using forskolin instead of light as a stimulus [53]. In accordance with our *in vivo* experiments (Fig. 6), expression of *Per1* but not *Per2* mRNA was induced in synchronized NIH 3T3 fibroblast cells after forskolin treatment (Supplementary Fig. 6d, e, blue bars). Comparable to the experiments in the SCN, *Per1* induction was abolished in *Cdk5* knock-out cells (Supplementary Fig. 6d). In contrast, *cFos* mRNA induction was not affected in *Cdk5* knock-out cells (Supplementary Fig. 6f), which is consistent with our observations in the SCN (Fig. 6g).

Collectively, our expression data provide evidence that *Cdk5* regulates light and forskolin-mediated expression of genes critical for the regulation of phase delays of the circadian clock. Immediate early genes, such as *Egr1*, are regulated in a similar manner, whereas others, such as *cFos*, are regulated by another mechanism not involving *Cdk5*.

Discussion

In this study, we investigated the role of Cdk5 in rapid phase shifts of the circadian clock. We found that Cdk5 activity is regulated by light and that Cdk5 is necessary for phase delays but not phase advances. We identified Cdk5 to play a major role in the modulation of Ca^{2+} levels and gating of the PKA-CaMK-CREB signaling pathway and coordinate it with the presence of PER2 in the nucleus of SCN cells.

In a previous study, we identified the protein kinase Cdk5 to regulate the phosphorylation and nuclear localization of the clock protein PER2 [34]. Because PER2 and protein kinases are involved in the photic signaling mechanism of clock phase adaptation [15, 20, 62, 70, 71], we tested the involvement of Cdk5 in this process. The phenotype of *Cdk5* knock-down (shCdk5) in the SCN of mice resembled the phenotypes observed in *Per2* mutant (*Per2*^{Brdm1}) and neuronal *Per2* knock-out (n*Per2* ko) mice. ShCdk5, as well as *Per2*^{Brdm1} and n*Per2* ko animals, showed strongly reduced phase delays in response to a short light pulse given at ZT14 (Fig. 1a, c) [20] or CT14 (Fig. 1d, f) [21, 72]. These mouse lines displayed a shortened period consistent with previous observations (Fig. 1b, e) [34, 73]. Our results indicate that Cdk5 is not only involved in the regulation of the circadian clock mechanism via nuclear localization of PER2 but also plays an important role in the molecular mechanism that leads to a delay of clock phase in response to a light pulse in the early dark phase or early subjective night.

Since Cdk5 mediates the effects of light at the behavioral (Fig. 1) level, we tested the influence of light on Cdk5 protein accumulation and kinase activity in the SCN at ZT14 (Fig. 2). We observed no change in the protein accumulation of Cdk5. On the other hand, Cdk5 kinase activity was reduced in the SCN after a light pulse at ZT14 (Fig. 2d, e) which was surprising in the context of increased p35 levels (Fig. 2a, c) and augmented PKA phosphorylation (Fig. 2a, b). However, this observation is in line with what we previously

reported, where we demonstrated that Cdk5 kinase activity was low during the light phase and higher during the dark phase [34]. It appeared, however, that p35 was not interacting with Cdk5 after light at ZT14 (Fig. 2f). Additional interactions of Cdk5 with unknown proteins may also be lost (Supplementary Fig. 2c). These observations suggest that Cdk5 was most likely modified in response to light leading to loss of interaction with p35 and other proteins. Ser159 of Cdk5 mediates the specificity of the Cdk5-p35 interaction [74], and therefore, phosphorylation of this site by an unknown kinase may mediate the loss of Cdk5 activity. Several additional phosphorylation sites in Cdk5 have been identified, of which phosphorylation of S47 renders Cdk5 inactive [75]. Which one of the phosphorylation sites in Cdk5 is modulated by light and what additional interactors may be involved in this process remains to be established.

Light in the early portion of the dark phase elicits phase delays, which involve T-type calcium channels, PKA-signaling, and Ca^{2+} signaling, ending in the phosphorylation of CREB (reviewed in [62]). We observed that in shCdk5 mice, CREB was already phosphorylated in the absence of light, although the total protein amount did not change (Fig. 3a, Supplementary Fig. 3a, b). Similarly, CaMKII and CaMKIV were shown to be phosphorylated and, therefore, activated only after the light pulse in control animals (Fig. 3b, d). Conversely, these kinases were highly phosphorylated in a light-independent manner in the SCN of shCdk5 animals (Fig. 3b, d) indicating that Cdk5 had a suppressive function on the phosphorylation of CaMKII and CaMKIV.

A stimulus can promote calmodulin (CAM) involving CaMKII gamma to translocate from calcium channels to the nucleus to promote CaMKIV phosphorylation and activation [44]. Unexpectedly, we observed that a light stimulus can have a similar but distinct effect on CAM in SCN cells (Fig. 3c). CaMKII alpha was phosphorylated after a light pulse at ZT14, which lead to perinuclear localization of CAM in control mice, while this localization pattern was already observed in shCdk5 animals independently of the light stimulus (Fig. 3c). In control mice that received no light CAM showed a diffuse expression pattern similar to the T-type calcium channel Cav3.1 at ZT14.

Interestingly, this light driven localization pattern was echoed by the change in cellular distribution of the T-type calcium channel Cav3.1 known as internalization/externalization. Again, the presence of Cdk5 suppressed the localization of this channel to the cell membrane in the absence of light, with light allowing localization to the cell membrane (Fig. 3e). This observation is reminiscent of investigations described previously in which Cdk5 appeared to play an important role in channel translocation [76, 77] as well as in receptor translocation [46, 47]. Thus, our findings are in accordance with the view that Cdk5 plays a crucial role in light stimulus driven cell dynamics.

Calcium plays an important role in circadian and phase-shifting biology [48]. Circadian calcium fluxes in the cytosol of SCN neurons have been demonstrated *in vitro* [78] and they change rapidly as a response to light perceived by the retina [49]. We performed *in vivo* live imaging to detect Ca^{2+} levels in the SCN using fiber photometry with protein-based Ca^{2+} indicators such as GCaMP [79]. With this approach, we observed that calcium fluxes in the SCN of control mice increased during and after a light pulse, but this change was significantly dampened in shCdk5 animals (Fig. 4b, c). Interestingly, although the Ca^{2+} influx was generally reduced in the SCN of shCdk5 mice, we observed random Ca^{2+} activity, which were independent of any light stimulus. These transients were observed also at the beginning of ZT14, before the light pulse (Fig. 4b, c). These results may indicate the presence of a calcium leak reminiscent of the already active phosphorylation cascade observed in the shCdk5 SCN in the absence of light (Fig. 3). We do not know, however, whether internal calcium stores involving ryanodine receptors [80] are altered by Cdk5 as well and how this would contribute to the observed phenotypes.

The PKA signaling pathway is involved in the resetting of the circadian phase (reviewed in [50]). Interference with PKA activation in the early subjective night led to reduced phase delay responses as observed *in vitro* in the SCN [52]. Here we find that Cdk5 plays an inhibitory role in PKA phosphorylation and activation. The FRET approach shows that in cells the lack of Cdk5 makes cells unresponsive to forskolin (Fig. 5a), an agent known to mitigate phase shifts in cells via PKA [53]. Interestingly, PKA appears to influence phase shifts and CREB phosphorylation indirectly via a Ca^{2+} dependent mechanism (Fig. 5b) with phosphorylated CaMKIV being the kinase that phosphorylates CREB (Supplementary Fig. 5b, c). This observation is in contrast with previous studies that suggested a direct phosphorylation of CREB by PKA [10, 52]. However, p-PKA is mostly located in the cytoplasm (Fig. 5e) while p-CaMKIV is in the nuclei (Fig. 3d). Furthermore, our experiments indicate that CREB did not interact with p-PKA but did with p-CaMKIV (suppl Fig. 5b, c), supporting the notion that PKA regulates CREB phosphorylation indirectly via CaMKIV in the SCN.

Because we observed that PKA was already phosphorylated in the dark when Cdk5 was silenced (Fig.5e), we asked how Cdk5 could negatively regulate PKA phosphorylation. A previous study described that Cdk5 can phosphorylate DARPP32 to suppresses PKA activity [81]. Furthermore, *Darpp-32* KO mice show attenuated phase delays [12] resembling shCdk5 mice (Fig. 1). In accordance with these studies, we found an inverse correlation between p-DARPP32 (Fig. 5d) and p-PKA (Fig. 5e), implying that Cdk5 indirectly inhibits PKA activity via DARPP32.

Our results imply that PKA action on CREB might be mediated via T-type calcium channels such as Cav 3.1 (Fig. 5f). This assumption is reasonable because PKA can phosphorylate Cav 3.1 channels and increase electrical conductivity, which leads to a higher influx of Ca^{2+} [26]. To that extent, our results indicate that a higher co-localization of p-PKA with Cav 3.1 is associated with an activation of the CaMKinase pathway and CREB phosphorylation.

Light induced phosphorylation of CREB leads to induction of immediate early genes and clock genes (reviewed in [62]). Accordingly, we observed that the clock genes *Per1* and *Dec1* but not *Per2*, *Dec2*, and *Bmal1* were induced in the SCN by light at ZT14 (Fig. 6a-e, blue bars) consistent with previous findings [15, 18, 61, 63]. The light induction of *Per1* and *Dec1* was abolished in shCdk5 animals (Fig. 6a, c, red bars) as well as in $Per2^{Brdm1}$ mutant mice (Supplementary Fig. 6b, c), suggesting involvement of Cdk5 and Per2 in induction of these genes. In contrast, light induction of the immediate early gene *cFos* was neither affected in shCdk5 nor $Per2^{Brdm1}$ SCN (Fig. 6g, Supplementary Fig. 6f), resembling the normal *cFos* induction in *Per2* KO animals [15]. This indicates that the light signaling mechanism for *cFos* induction is different from the one mediating induction of *Per1* and *Dec1*. Interestingly, however, the light-inducible genes *Sik1* and *Gem*, which are involved in limiting the effects of light on the clock [68, 69] were not light-inducible in shCdk5 animals (Fig. 6i, j) supporting the view that the factors that drive (*Per1*, *Dec1*) or limit (*Sik1*, *Gem*) the effects of light on the clock are regulated by the same mechanism. Interestingly, neither lack of *Per1*, *Dec1* [20, 82] nor *Sik1* or *Gem* [68, 69] alone abolish phase delays. Of note is that lack of *cFos* or *Egr1* did not affect phase delays either [83, 84]. Furthermore, the neuropeptide vasoactive intestinal peptide (VIP), which is important in circadian light responses [67], was not inducible by a light pulse at ZT14 in control as well as shCdk5 animals (Supplementary Fig. 6a), indicating that Cdk5 acts upstream of VIP signaling. Overall, our data suggest that Cdk5 not only regulates the light sensitive PKA – CaMK- CREB signaling pathway but ultimately also affects gene expression. The combination of lack of induction of many genes in the Cdk5-regulated pathway is responsible for the manifestation of rapid behavioral phase delays.

Based on this and our previous studies, we propose the following molecular model for light-mediated phase delays (Fig. 7). The model is divided into two parts. One part describes the state before the light pulse, and the second part the mechanism after the light pulse. The state before the light pulse (ZT12-14) is depicted in the gray area in Figure 7. As reported previously, Cdk5 is active right after dark onset [34], depicted as the active Cdk5/p35 complex (blue). This has two consequences: 1) PER2 (red) is phosphorylated and translocates to the nucleus [34], and 2) DARPP32 is phosphorylated and thus inhibiting PKA activity [81]. Hence, before the light pulse at ZT14, the nucleus is supplied with PER2, which appears to be necessary for light-mediated behavioral phase delays [20, 21, 72]. In parallel, the signaling pathway necessary to phosphorylate CREB is turned off. This state can then be dramatically changed when light is applied at ZT14 evoking glutamate and PACAP release at the synapses between the RHT and the SCN. Interaction between p35 and Cdk5 is abolished (Fig. 2) thereby inactivating Cdk5 and stopping phosphorylation of PER2 and DARPP32. Since significant amounts of PER2 are already in the nucleus this probably has no consequences on nuclear PER2 function. However, DARPP32 is not phosphorylated anymore and the block on PKA is released. At the same time, PKA becomes phosphorylated due to PACAP and cAMP signaling, leading to activation of Cav3.1 by PKA (Fig. 5f, [26]). This leads to CaMKII and CaMKIV phosphorylation and, ultimately, to the phosphorylation of CREB in the nucleus (Fig. 3, [45]). Phospho-CREB builds up a complex with CRTC1/CBP and PER2 [15] to activate gene expression of the *Per1*, *Dec1*, *Sik1*, and *Gem* genes. In the activation complex the amount of PER2 present in the nucleus may at least in part affect the magnitude of the phase delay, which is depending on the time the light pulse is given. In conclusion, Cdk5 activity is gating both processes, the pre-light condition as well as the post-light condition, leading to a concerted activation of a set of light-responsive genes that impinge on behavioral phase delays in response to nocturnal light exposure.

Methods

Animals and housing

All mice were housed with chow food (3432PX, Kliba-Nafag) and water ad libitum in transparent plastic cages (267 mm long, ×207 mm wide, ×140 mm high; Techniplast Makrolon type 2 1264C001) with a stainless-steel wire lid (Techniplast 1264C116), kept in soundproof ventilated chambers at constant temperature (22 ± 2 °C) and humidity (40 – 50%). All mice were entrained to a 12-h light–dark cycle (LD cycle), and the time of day was expressed as Zeitgeber time (ZT; ZT0 lights on, ZT12 lights off). Four-month-old 129/C57BL6 mixed males were used for the experiments. Housing and experimental procedures were performed per the guidelines of the Schweizer Tierschutzgesetz and the declaration of Helsinki. The state veterinarians of the Canton of Fribourg and Bern approved the protocol (license numbers: 2021-19-FR; BE45/18; BE21/22).

Locomotor activity monitoring

Locomotor activity parameters were analyzed by monitoring wheel-running activity, as described in [85], and calculated using the ClockLab software (Actimetrics). To analyze free-running rhythms, animals were entrained to LD 12:12 and released into constant darkness (DD). The internal period length was determined from a regression line drawn through the activity onsets of ten days of stable rhythmicity under constant conditions, calculated using the respective inbuilt functions of the ClockLab software (Acquisition Version 3.208, Analysis Version 6.0.36). For better visualization of daily rhythms, locomotor activity records were double-plotted, which means that each day's activity is plotted twice, to the right and below that of the previous day. For the analysis of light-induced resetting, we used an Aschoff type II and I protocol [85]. For type II, mice maintained in LD 12:12 were subjected to a 15 min. light pulse (LP, 500 lux) at ZT10 (no phase shift), 14 (phase delay), and 22 (phase advance). Subsequently, they were released into DD for ten days, and phase shift was measured. For type I, mice maintained in DD were subjected to a 15 min. light pulse at Circadian Time (CT) 10, 14, or 22. A circadian hour equals 1/24 of the endogenous period (τ), calculated as follows: circadian hour = tau/24 hours. To convert ZT hours to CT hours, we multiply the circadian hour by the actual hours needed to apply the light pulse at a specific time [i.e., CT14= (tau/24 hours) *14]. The phase shift was determined by fitting a regression line through the activity onsets of at least 7 days under LD conditions before the light pulse and a second line through the activity onsets of at least 7 days under DD after the light pulse. The first two days after the administration of the light pulse were not considered for the calculation of the phase shift. The distance between the two regression lines determined the phase shift. Before starting any new protocol, mice were allowed to stabilize their circadian oscillator for 10 days. The corresponding figure legends indicate the number of animals used in the behavioral studies.

Light pulse and tissue isolation

Light pulse (LP., 500 lux) was given at ZT14, and mice were sacrificed at appropriate indicated times. Brains were collected, and SCN tissue was isolated for western blot or RT-qPCR use. For immunofluorescence experiments, mice were perfused with 4% PFA and cryoprotected in 30% sucrose. Tissue isolation at ZT14 without a light pulse was used as light-induction negative control.

RNA extraction and cDNA synthesis

Total RNA was extracted from confluent 6 cm petri dishes or frozen SCN tissue using the Microspin RNA II kit (Machery & Nagel, Düren, Germany) according to the manufacturer's instructions. 0.5 μg of total RNA was converted to single-strand cDNA in a total volume of

10 µL using the SuperScript IV VILO kit (Thermo Fisher Scientific, Waltham MA, USA) according to the manufacturer's instructions. The samples were diluted to 200 µL with pure water. 5 µL of each sample were mixed with 7.5 µL of KAPA probe fast universal real-time PCR master mix (Merck, Darmstadt, Germany) and 2.5 µL of the indicated primer/probe combinations. For the subsequent real-time PCR, a Rotorgene 6000 machine was used (Qiagen, Hilden, Germany) and analyzed with the propriety software.

qPCR primers

Per1:

FW: GGC ATG ATG CTG CTG ACC ACG
RV: ACT GGG GCC ACC TCC AGT TC
TM: FAM-TGG CCC TCC CTC ACC TTA GCC TGT TCC T-BHQ1

Per2:

FW: TCC ACA GCT ACA CCA CCC CTT A
RV: TTT CTC CTC CAT GCA CTC CTG A
TM: FAM-CCG CTG CAC ACA CTC CAG GGC G-BHQ1

Dec1

FW: TGC AGA CAG GAG CGC ACA GT
RV: GCT TTGGGC AGG CAG GTA GGA
TM: FAM-TGG TTG CGC GCT GGG GAT CCG T-BHQ1

Dec2

FW: ACA GAA TGG GGA GCG CTC TCT GAA
RV: TGA AAC CCC GAG TGG AAC GCA
TM: FAM-CGC CGG TCC AGG CCG ACT TGG A-BHQ1

Bmal1

FW: GCA ATG CAA TGT CCA GGA AG
RV: GCT TCT GTG TAT GGG TTG GT
TM: FAM- ACC GTG CTA AGG ATG GCT GTT CAG CA-BHQ1

eGFP

FW: CAT CTG CAC CAC CGG CAA GC
RV: GGT CGG GGT AGC GGC TGA A
TM: FAM- TGC CCG TGC CCT GGC CCA CC-BHQ1

cFos

FW: GCC GGG GAC AGC CTT TCC TA
RV: TCT GCG CAA AAG TCC TGT GTG TTG A
TM: FAM-CCA GCC GAC TCC TTC TCC AGC ATG GGC-BHQ1

Egr1

FW: CGG CAG CAG CGC CTT CAA T
RV: GGA CTC TGT GGT CAG GTG CTC AT
TM: FAM-CCT CAA GGG GAG CCG AGC GAA CAA CCC-BHQ1

Sik1

FW: GGC TGC ACG ACC AGC AAT CG
RV: GGC GGT AGA AGA GTG GTG CTG TA
TM: FAM- TCC TGC ACC AGC AGA GGC TGC TCC AG-BHQ1

Gem

FW: TGG GAA AAT AAG GGG GAG AA
RV: AGC TTG CAC GGT CTG TGA TA
TM: FAM- CCA CTG CAT GCA GGT CGG GGA TGC C-BHQ1

Vip

FW: AGC AGA ACT TCA GCA CCC TAG ACA
RV: TCG GTG CCT CCT TGG CTG TT
TM: FAM- AGC CGG AAA GGC AGC CCT GCC T-BHQ1

Tprkb (normalisation probe for Tprkb)

FW: GGC TGG CAT CAG ACC CAC AGA
RV: GGG CCC GTA GAG TCG GGA AA
TM: FAM-CCT GCG TCT GCC CTC TGA GGG CTG-BHQ1

Atp5h (normalisation probe for Atp5h)

FW: TGC CCT GAA GAT TCC TGT GCC T
RV: ACT CAG CAC AGC TCT TCA CAT CCT
TM: FAM-TCT CCT CCT GGT CCA CCA GGG CTG TGT-BHQ1

Sirt2 (normalisation probe for Sirt2)

FW: CAG GCC AGA CGG ACC CCT TC
RV: AGG CCA CGT CCC TGT AAG CC
TM: FAM- TGA TGG GCC TGG GAG GTG GCA TGG A-BHQ1

Nono (normalisation probe for Nono)

FW: TCT TTT CTC GGG ACG GTG GAG
RV: GTC TGC CTC GCA GTC CTC ACT
TM: FAM- CGT GCA GCG TCG CCC ATA CTC CGA GC-BHQ1

Immunofluorescence

SCN cryosections (40 µM) were placed in a 24-well plate, washed three times with 1x TBS (0.1 M Tris/0.15 M NaCl) and 2x SSC (0.3 M NaCl/0.03 M tri-Na-citrate pH 7). Antigen retrieval was performed with 2xSSC heating to 85°C for 30 min. Then, sections were washed twice in 2x SSC and three times in 1x TBS pH 7.5 before blocking them for 1.5 hours in 10% fetal bovine serum (Gibco)/0.1% Triton X-100/1x TBS at RT. If the recipient species for some raised antibody was the mouse, we performed a Mouse on Mouse (MOM; Ab269452) blocking (2h) before 10% FBS to block endogenous mouse immunoglobulins in a mouse tissue section. After the blocking, the primary antibodies (Table 1), diluted in 1% FBS/0.1% Triton X-100/1x TBS, were added to the sections and incubated overnight at 4°C. The next day, sections were washed with 1x TBS and incubated with the appropriate fluorescent secondary antibodies diluted 1:500 in 1% FBS/0.1% Triton X-100/1x TBS for 3 hours at RT. (Alexa Fluor 488-AffiniPure Donkey Anti-Rabbit IgG (H+L) no. 711–545–152, Lot: 132876, Alexa Fluor647-AffiniPure Donkey Anti-Mouse IgG (H+L) no. 715–605–150, Lot: 131725, Alexa Fluor647-AffiniPure Donkey Anti-Rabbit IgG (H+L) no. 711–602–152, Lot: 136317 and all from Jackson Immuno Research). Tissue sections were stained with DAPI (1:5000 in PBS; Roche) for 15 min. Finally, the tissue sections were rewashed twice in 1x TBS and mounted on glass microscope slides. Fluorescent images were taken using a confocal microscope (Leica TCS SP5), and pictures were taken with a magnification of 63x with or without indicated additional zoom. Images were processed with the Leica Application Suite Advanced Fluorescence 2.7.3.9723. Immunostained sections were quantified using ImageJ version 1.49. Statistical analysis was performed on three animals per treatment.

Antibody	Specie	Company	Catalog number	Dilution
anti-Cdk5 clone 2H6	Mouse	Origene	CF500397	1:100
anti-GFP	Rabbit	Abcam	ab6556	1:500
Anti-Creb	Rabbit	Cell signaling	D76D11	1:200
Anti-Creb (pSer133)	Rabbit	Abcam	Ab32096	1:500
Anti-CaMKII	Rabbit	Abcam	Ab52470	1:200
Anti-CaMKII (pThr286)	Mouse	Invitrogen	MA1-047	1:100
Anti-CaMKIV	Rabbit	Abcam	Ab3557	1:200
Anti-CaMKIV (pThr196/200)	Rabbit	Invitrogen	PA5-105011	1:100
Anti-CaV3.1	Rabbit	Invitrogen	PA5-50635	1:100
Anti-Calmodulin	Mouse	Invitrogen	MA3-917	1:100
Anti-PKA (pT197)	Rabbit	Abcam	Ab75991	1:100
Anti-Darpp32 (pThr75)	Rabbit	Invitrogen	PA5-105037	1:100

Table 1. Antibodies used for the immunostainings.

Adeno Associated Virus (AAV) production and stereotaxic injections

Experiments were performed as previously described [34]. Stereotaxic injections were performed on 4- to 5-month-old mice under isoflurane anesthesia using a stereotaxic

apparatus (Stoelting). The brain was exposed by craniotomy, and the Bregma was used as a reference point for all coordinates. AAVs were injected bilaterally into the SCN (Bregma: anterior-posterior (AP) − 0.40 mm; medial-lateral (ML) ±0.00 mm; dorsal-ventral (DV) – 5.7 mm, angle + /- 3°) using a hydraulic manipulator (Narishige: MO-10 one-axis oil hydraulic micromanipulator, http://products.narishige-group.com/group1/MO-10/electro/english.html) at a rate of 40 nL/min through a pulled glass pipette (Drummond, 10 µl glass micropipette; Cat number: 5-000-1001-X10). The pipette was first raised 0.1 mm to allow the spread of the AAVs and later withdrawn 5 min after the end of the injection. After surgery, mice were allowed to recover for 2 weeks and entrained to LD 12:12 before behavior and molecular investigations.
The injected viruses were:

- SsAAV-9/2-hSyn1-chI[mouse(shCdk5)]-EGFP-WPRE-SV40p(A)
- ssAAV-9/2-hSyn1-chI[1x(shNS)]-EGFP-WPRE-SV40p(A)

Protein extraction from SCN tissue.

The protocol was a modified version of what was published before [15]. Isolated SCNs obtained from 4 different mice were pooled according to the indicated condition (either dark or 15 min after the light pulse). The pooled tissues were frozen in liquid N2 and resuspended in a brain-specific lysis buffer (50 mM Tris-HCl pH 7.4, 150 mM NaCl, 0.25% SDS, 0.25% sodium deoxycholate, 1 mM EDTA). They were homogenized using a pellet pestle, kept on ice for 30 min and vortexed for 30 s, followed by N2 freezing. Frozen samples were left to melt on ice. The samples were sonicated (10 s, 15% amplitude) and centrifuged for 20 min at 16,000 g at 4 °C. The supernatant was collected in new tubes, and the pellet was discarded.

Immunoprecipitation.
The protocol was described before [34]. The protein extract was diluted with the appropriate lysis buffer in a final volume of 250 µL and immunoprecipitated using the indicated antibody (ratio 1:50). The reaction was kept at 4°C overnight on a rotary shaker. The day after, samples were captured with 50 µL of 50% (w/v) protein-A agarose beads (Roche), and the reaction was kept at 4°C for 3 hr on a rotary shaker. Before use, beads were washed thrice with the appropriate protein buffer and resuspended in the same buffer (50% w/v). The beads were collected by centrifugation and washed three times with NP-40 buffer (100 mM Tris-HCl pH7.5, 150 mM NaCl, 2 mM EDTA, 0.1% NP-40). After the final wash, beads were resuspended in 2% SDS 10%, glycerol, 63 mM Trish-HCL pH 6.8, and proteins were eluted for 15 min at RT. Laemmli buffer was finally added, and samples were boiled for 5 min at 95° C and loaded onto 10% SDS-PAGE gels.

Western blot.
Circa 40 µg o of protein was loaded onto 10% SDS-PAGE gel and run at 100 Volt for two hours. Protein migration was followed by a semidry transfer (40 mA, 1 h 30 s) using Hybond® ECL™ nitrocellulose. We subsequently performed red ponceau staining (0.1% of Ponceau S dye and 5%) on the membrane to confirm the successful transfer. The list of antibodies used in the paper is shown in Table 2. The membrane was washed with TBS 1x/Tween 0.1% and blocked with TBS 1x/BSA 5%/Tween 0.1% for 1 h. After washing, the membrane was blotted with the appropriate primary antibodies overnight. The day after, membranes were washed three times with TBS 1x/Tween 0.1%, followed by secondary

antibody immunoblotting for 1 h at room temperature. The densitometric signal was digitally acquired with the Azure Biosystem.

Antibody	Specie	Company	Catalog number	Dilution
anti-Cdk5	Rabbit	Cell signaling	D1F7M	1:3000
Anti-Creb	Rabbit	Cell signaling	D76D11	1:3000
Anti-Creb (pSer133)	Rabbit	Abcam	Ab32096	1:1000
Anti-PKA (pT197)	Rabbit	Abcam	Ab75991	1:1000
Anti-p35	Rabbit	Invitrogen	MA5-14834	1:1000
Anti-CaMKIV (pThr196/200)	Rabbit	Invitrogen	PA5-105011	1:1000

Table 2. Antibodies used for the western blots.

***In vitro* kinase assay using immunoprecipitated Cdk5 from SCN.**
The protocol is the same as before [34]. CDK5 was immunoprecipitated (4°C overnight with 2x Protein A agarose (Sigma-Aldrich)) from SCN samples at ZT14 in the dark or after a light pulse (LP., circa 500 lux) of 15min. After immunoprecipitation, samples were diluted in a washing buffer and split into two halves. One-half of the IP was used for an *in vitro* kinase assay. Briefly, 1 µg of histone H1 (Sigma-Aldrich) was added to the immunoprecipitated CDK5. Assays were carried out in reaction buffer (30 mM HEPES, pH 7.2, 10 mM $MgCl_2$, and 1 mM DTT) containing [γ-^{32}P] ATP (10 Ci) at 30°C for 1 hour and then terminated by adding SDS sample buffer and boiling for 5 min. Samples were subjected to 15% SDS-PAGE, stained by Coomassie Brilliant Blue, and dried, and then phosphorylated histone H1 was detected by autoradiography. The other half of the IP was used for Western blotting to determine the total CDK5 immunoprecipitated from the SCN samples. The following formula was used to quantify the kinase activity at each time point: ([^{32}P] H1/total H1)/CDK5 $^{\text{IP protein}}$.

Cell Culture
NIH3T3 wt and CRISPR/Cas9 *Cdk5* ko [34] mouse fibroblast cells (ATCCRCRL-1658) were maintained in Dulbecco's modified Eagle's medium (DMEM), containing 10% fetal calf serum (FCS) and 100 U/mL penicillin-streptomycin at 37°C in a humidified atmosphere containing 5% CO2. For any experiment, cells were synchronized with forskolin (100 µM).

Surgical procedure for fiber photometry recordings
Animals previously infected either with AAV9-hSyn1-chI[1x(shNS)]-jGCaMP7b-WPRE-SV40p(A) (*scramble*) or AAV9-hSyn1-chI[mouse(shCdk5)]- jGCaMP7b -WPRE-SV40p(A) (*shCDK5*), were injected with Metacam (Meloxicam, 5mg/kg s.c.) for analgesia, then anesthetized with 1.5 –2 % isoflurane/O_2 mix. Mice were placed in a Kopf digital stereotactic frame. Their body temperature was kept constant at 37 °C via a feedback-coupled heating device (Panlab/Harvard Apparatus), and their eyes were covered with ointment (Bepanthen Augen- und Nasensalbe, Bayer). After the skin incision (formerly prepared aseptically), the skull bone was cleaned with saline to remove the remaining tissue. A small craniotomy to target the SCN was drilled into the skull (Micro-Drill from Harvard Apparatus with burrs of 0.7 mm diameter from Fine Science Tools), and the dura was carefully removed. An optical

fiber implant (400 µm, 0.5 NA Core Multimode Optical Fiber, FT400ERT, inserted into ceramic ferrules, 2.5 mm OD; 440 µm ID, Thorlabs) was slowly implanted above the SCN to allow for imaging of GCaMP7b signals (AP: +0.40; ML: ±0.0; DV: -5.3; angle +/- 4°). One stainless steel screw was inserted into the skull over the cerebellum for stability purposes. The implant was then secured to the skull with dental cement (Paladur, Kulzer). After surgical procedures, mice were allowed to recover for one week and finally tethered with an optical patch cord.

Fiber photometry experimental design.

GCaMP7b was excited with a blue LED (Doric, LED driver, assembled with 470 nm) at 480 Hz, and emission was sampled at 2'000 Hz with a photodetector (Doric, DFD_FPA_FC) through a fluorescence MiniCube (Doric, ilFMC6_IE(400-410)_E1(460-490)_F1(500-540)_E2(555-570)_F2(580-680)_S) and digitized with a national instruments USB-6002 DAQ device. Fiber photometry recordings were acquired using custom-written scripts in LabVIEW on a computer. All the recordings were started about 15 min before ZT14 to stabilize the fluorescent signal. For every trial at ZT14 a constant light pulse of 10000 Lux (Daylight Lamp) was manually turned on for 15 min (± 20 seconds), and the recording was stopped 15 minutes after the light was switched off. To allow mice to restore their circadian time to the 12-h light–dark cycle, the intertrial interval was of minimum 10 days. In order to align the light pulse to the photometry recording, a patch cord was connected to the light source and the photometry system

In vivo calcium imaging, data processing and analysis

The data were subdivided into control (*scramble*) and experimental (*shCDK5*) groups. The fluorescent signal was demodulated in the frequency band of 470 – 490 Hz at 10 Hz acquisition rate. Due to GCaMP7b variable photobleaching (i.e., the loss of fluorescence intensity as a function of light exposure), we filtered the demodulated signal using a 3 order Savitzky-Golay filter (every 100 s), and detrended it using a hug-line. We then calculated the $\Delta F/F_0$ as follows:

$$\frac{\Delta F}{F_0} = \frac{detrended\ signal - 1^{st}\ percentile(detrended\ signal)}{99^{th}\ percentile(detrended\ signal) - 1^{st}\ percentile(detrended\ signal)}$$

Finally, the $\Delta F/F_0$ was cut to the light pulse as follow: 5 minutes before light pulse, light pulse period and 15 minutes after the light. To exclude differences in the duration of the light pulse (± 20 seconds), the period analyzed was of 14 minutes. All data processing was performed using custom-written Matlab scripts.

Live FRET imaging

The protocol was performed as before [15]. The following plasmid was used for the project**:** ICAP-NLS Vector carrying [15]. Transfected NIH3T3 cells were starved for 4 h with 0.5% FBS DMEM. Subsequently, cells were washed twice with 1×HBTS without CaCl2 and MgCl2 (25 mM HEPES, 119 mM NaCl, 6gr/L Glucose, 5 mM KCl) and resuspended in the same buffer. NIH3T3 cells were imaged using an inverted epifluorescence microscope (Leica DMI6000B) with an HCX PL Fluotar 5x/0.15 CORR dry objective, a Leica DFC360FX CCD camera (1.4 M pixels, 20 fps), and EL6000 Light Source, and equipped with fast filter wheels for FRET imaging. Excitation filters for CFP and FRET: 427 nm (BP 427/10). Emission filters for CFP: 472 (BP 472/30) and FRET: 542 nm (BP 542/27). Dichroic mirror: RCY 440/520. One frame every 20 sec was acquired for at least 90 cycles (0.05 Hz frequency), and

the recording lasted at least 30 min. The baseline response in the presence of HBTS was recorded for 2 min and 40s. At minute 3:00, 100 µM Forskolin, 2 mM CaCl2, and 2 mM MgCl2 were added to the cells. The time-lapse recordings were analyzed using LAS X software (Leica). Two regions of interest (ROI) were randomly selected for each cell, and 50 cells per plate were chosen randomly. A first ROI delimiting the background and a second ROI including the cell nucleus of NIH3T3 cell expressing NLS KIDKIX were used per cell. The ROI background values were subtracted from the ROI cell values for each channel. For baseline normalization, the FRET ratio R was expressed as a ΔR/R, where ΔR is R–R0, and R0 is the average of R over the last 120 s prior stimulus.

Statistical analysis

Statistical analysis of all experiments was performed using GraphPad Prism6 software. Depending on the data type, either an unpaired t-test or one- or two-way ANOVA with Bonferroni or Tukey's post-hoc test was performed. Values considered significantly different are highlighted. [$p<0.05$ (*), $p<0.01$ (**), or $p<0.001$ (***)].

Data were compared via two-way repeated-measures ANOVA with post hoc Bonferroni's corrections for multiple comparisons. Data distribution was assumed to be normal, but this was not formally tested. All data are displayed as mean ± standard error of the mean (SEM). No power calculations were performed to determine sample sizes, but similarly sized cohorts were used in previous studies. The experimenters were not blind to the conditions when acquiring or analyzing the data.

Sample numbers are indicated in the corresponding figure legends, and test details are only reported for significant results. Figures were prepared in Adobe Illustrator 2022.

References

1. Roenneberg T, Merrow M. The Circadian Clock and Human Health. *Curr Biol* **26**, R432-443 (2016).
2. Hastings MH, Maywood ES, Brancaccio M. The Mammalian Circadian Timing System and the Suprachiasmatic Nucleus as Its Pacemaker. *Biology (Basel)* **8**, (2019).
3. Takahashi JS. Transcriptional architecture of the mammalian circadian clock. *Nat Rev Genet* **18**, 164-179 (2017).
4. Hirano A, Fu YH, Ptacek LJ. The intricate dance of post-translational modifications in the rhythm of life. *Nat Struct Mol Biol* **23**, 1053-1060 (2016).
5. Partch CL. Orchestration of Circadian Timing by Macromolecular Protein Assemblies. *J Mol Biol* **432**, 3426-3448 (2020).
6. Allen CN, Nitabach MN, Colwell CS. Membrane Currents, Gene Expression, and Circadian Clocks. *Cold Spring Harb Perspect Biol* **9**, (2017).
7. LeGates TA, Fernandez DC, Hattar S. Light as a central modulator of circadian rhythms, sleep and affect. *Nat Rev Neurosci* **15**, 443-454 (2014).
8. Ding JM, Chen D, Weber ET, Faiman LE, Rea MA, Gillette MU. Resetting the biological clock: mediation of nocturnal circadian shifts by glutamate and NO. *Science* **266**, 1713-1717 (1994).
9. Obrietan K, Impey S, Storm DR. Light and circadian rhythmicity regulate MAP kinase activation in the suprachiasmatic nuclei. *Nat Neurosci* **1**, 693-700 (1998).
10. Ginty DD, *et al.* Regulation of CREB phosphorylation in the suprachiasmatic nucleus by light and a circadian clock. *Science* **260**, 238-241 (1993).
11. Gau D, *et al.* Phosphorylation of CREB Ser142 regulates light-induced phase shifts of the circadian clock. *Neuron* **34**, 245-253 (2002).
12. Yan L, Bobula JM, Svenningsson P, Greengard P, Silver R. DARPP-32 involvement in the photic pathway of the circadian system. *J Neurosci* **26**, 9434-9438 (2006).
13. Wheaton KL, *et al.* The Phosphorylation of CREB at Serine 133 Is a Key Event for Circadian Clock Timing and Entrainment in the Suprachiasmatic Nucleus. *J Biol Rhythms* **33**, 497-514 (2018).
14. Crosio C, Cermakian N, Allis CD, Sassone-Corsi P. Light induces chromatin modification in cells of the mammalian circadian clock. *Nat Neurosci* **3**, 1241-1247 (2000).
15. Brenna A, Ripperger JA, Saro G, Glauser DA, Yang Z, Albrecht U. PER2 mediates CREB-dependent light induction of the clock gene Per1. *Sci Rep* **11**, 21766 (2021).
16. Rusak B, Robertson HA, Wisden W, Hunt SP. Light pulses that shift rhythms induce gene expression in the suprachiasmatic nucleus. *Science* **248**, 1237-1240 (1990).
17. Albrecht U, Sun ZS, Eichele G, Lee CC. A differential response of two putative mammalian circadian regulators, mper1 and mper2, to light. *Cell* **91**, 1055-1064 (1997).
18. Shigeyoshi Y, *et al.* Light-induced resetting of a mammalian circadian clock is associated with rapid induction of the mPer1 transcript. *Cell* **91**, 1043-1053 (1997).
19. Daan S, Pittendrigh CS. A functional analysis of circadian pacemakers in nocturnal rodents II. The variability of phase response curves. *J Comp Physiol* **106**, 253-266 (1976).
20. Albrecht U, Zheng B, Larkin D, Sun ZS, Lee CC. MPer1 and mper2 are essential for normal resetting of the circadian clock. *J Biol Rhythms* **16**, 100-104 (2001).
21. Spoelstra K, Albrecht U, van der Horst GT, Brauer V, Daan S. Phase responses to light pulses in mice lacking functional per or cry genes. *J Biol Rhythms* **19**, 518-529 (2004).

22. Catterall WA. Voltage-gated calcium channels. *Cold Spring Harb Perspect Biol* **3**, a003947 (2011).
23. Kim DY, *et al.* Voltage-gated calcium channels play crucial roles in the glutamate-induced phase shifts of the rat suprachiasmatic circadian clock. *Eur J Neurosci* **21**, 1215-1222 (2005).
24. Schmutz I, *et al.* A specific role for the REV-ERBalpha-controlled L-Type Voltage-Gated Calcium Channel CaV1.2 in resetting the circadian clock in the late night. *J Biol Rhythms* **29**, 288-298 (2014).
25. Perez-Reyes E. Molecular physiology of low-voltage-activated t-type calcium channels. *Physiol Rev* **83**, 117-161 (2003).
26. Kim JA, Park JY, Kang HW, Huh SU, Jeong SW, Lee JH. Augmentation of Cav3.2 T-type calcium channel activity by cAMP-dependent protein kinase A. *J Pharmacol Exp Ther* **318**, 230-237 (2006).
27. Chemin J, *et al.* Temperature-dependent modulation of CaV3 T-type calcium channels by protein kinases C and A in mammalian cells. *J Biol Chem* **282**, 32710-32718 (2007).
28. Calderon-Rivera A, Sandoval A, Gonzalez-Ramirez R, Gonzalez-Billault C, Felix R. Regulation of neuronal cav3.1 channels by cyclin-dependent kinase 5 (Cdk5). *PLoS One* **10**, e0119134 (2015).
29. Tang D, *et al.* An isoform of the neuronal cyclin-dependent kinase 5 (Cdk5) activator. *J Biol Chem* **270**, 26897-26903 (1995).
30. Tsai LH, Delalle I, Caviness VS, Jr., Chae T, Harlow E. p35 is a neural-specific regulatory subunit of cyclin-dependent kinase 5. *Nature* **371**, 419-423 (1994).
31. Brinkkoetter PT, *et al.* Cyclin I activates Cdk5 and regulates expression of Bcl-2 and Bcl-XL in postmitotic mouse cells. *J Clin Invest* **119**, 3089-3101 (2009).
32. Jessberger S, Gage FH, Eisch AJ, Lagace DC. Making a neuron: Cdk5 in embryonic and adult neurogenesis. *Trends Neurosci* **32**, 575-582 (2009).
33. Kawauchi T. Cdk5 regulates multiple cellular events in neural development, function and disease. *Dev Growth Differ* **56**, 335-348 (2014).
34. Brenna A, *et al.* Cyclin-dependent kinase 5 (CDK5) regulates the circadian clock. *Elife* **8**, (2019).
35. Ripperger JA, Chavan R, Albrecht U, Brenna A. Physical Interaction between Cyclin-Dependent Kinase 5 (CDK5) and Clock Factors Affects the Circadian Rhythmicity in Peripheral Oscillators. *Clocks Sleep* **4**, 185-201 (2022).
36. Ikegami K, Nakajima M, Minami Y, Nagano M, Masubuchi S, Shigeyoshi Y. cAMP response element induces Per1 in vivo. *Biochem Biophys Res Commun* **531**, 515-521 (2020).
37. Naruse Y, Oh-hashi K, Iijima N, Naruse M, Yoshioka H, Tanaka M. Circadian and light-induced transcription of clock gene Per1 depends on histone acetylation and deacetylation. *Mol Cell Biol* **24**, 6278-6287 (2004).
38. Travnickova-Bendova Z, Cermakian N, Reppert SM, Sassone-Corsi P. Bimodal regulation of mPeriod promoters by CREB-dependent signaling and CLOCK/BMAL1 activity. *Proc Natl Acad Sci U S A* **99**, 7728-7733 (2002).
39. Tischkau SA, Mitchell JW, Tyan SH, Buchanan GF, Gillette MU. Ca2+/cAMP response element-binding protein (CREB)-dependent activation of Per1 is required for light-induced signaling in the suprachiasmatic nucleus circadian clock. *J Biol Chem* **278**, 718-723 (2003).
40. Sheng M, Thompson MA, Greenberg ME. CREB: a Ca(2+)-regulated transcription factor phosphorylated by calmodulin-dependent kinases. *Science* **252**, 1427-1430 (1991).

41. Xing J, Ginty DD, Greenberg ME. Coupling of the RAS-MAPK pathway to gene activation by RSK2, a growth factor-regulated CREB kinase. *Science* **273**, 959-963 (1996).
42. Impey S, *et al.* Cross talk between ERK and PKA is required for Ca2+ stimulation of CREB-dependent transcription and ERK nuclear translocation. *Neuron* **21**, 869-883 (1998).
43. Yokota S, *et al.* Involvement of calcium-calmodulin protein kinase but not mitogen-activated protein kinase in light-induced phase delays and Per gene expression in the suprachiasmatic nucleus of the hamster. *J Neurochem* **77**, 618-627 (2001).
44. Ma H, *et al.* gammaCaMKII shuttles Ca(2)(+)/CaM to the nucleus to trigger CREB phosphorylation and gene expression. *Cell* **159**, 281-294 (2014).
45. Matthews RP, Guthrie CR, Wailes LM, Zhao X, Means AR, McKnight GS. Calcium/calmodulin-dependent protein kinase types II and IV differentially regulate CREB-dependent gene expression. *Mol Cell Biol* **14**, 6107-6116 (1994).
46. Liu J, Du J, Wang Y. CDK5 inhibits the clathrin-dependent internalization of TRPV1 by phosphorylating the clathrin adaptor protein AP2mu2. *Sci Signal* **12**, (2019).
47. Jeong J, *et al.* Cdk5 phosphorylates dopamine D2 receptor and attenuates downstream signaling. *PLoS One* **8**, e84482 (2013).
48. Colwell CS. NMDA-evoked calcium transients and currents in the suprachiasmatic nucleus: gating by the circadian system. *Eur J Neurosci* **13**, 1420-1428 (2001).
49. Irwin RP, Allen CN. Calcium response to retinohypothalamic tract synaptic transmission in suprachiasmatic nucleus neurons. *J Neurosci* **27**, 11748-11757 (2007).
50. Gillette MU, Mitchell JW. Signaling in the suprachiasmatic nucleus: selectively responsive and integrative. *Cell Tissue Res* **309**, 99-107 (2002).
51. Sterniczuk R, Yamakawa GR, Pomeroy T, Antle MC. Phase delays to light and gastrin-releasing peptide require the protein kinase A pathway. *Neurosci Lett* **559**, 24-29 (2014).
52. Tischkau SA, Gallman EA, Buchanan GF, Gillette MU. Differential cAMP gating of glutamatergic signaling regulates long-term state changes in the suprachiasmatic circadian clock. *J Neurosci* **20**, 7830-7837 (2000).
53. Yagita K, Okamura H. Forskolin induces circadian gene expression of rPer1, rPer2 and dbp in mammalian rat-1 fibroblasts. *FEBS Lett* **465**, 79-82 (2000).
54. Friedrich MW, Aramuni G, Mank M, Mackinnon JA, Griesbeck O. Imaging CREB activation in living cells. *J Biol Chem* **285**, 23285-23295 (2010).
55. Svenningsson P, Nishi A, Fisone G, Girault JA, Nairn AC, Greengard P. DARPP-32: an integrator of neurotransmission. *Annu Rev Pharmacol Toxicol* **44**, 269-296 (2004).
56. Yonemoto W, Garrod SM, Bell SM, Taylor SS. Identification of phosphorylation sites in the recombinant catalytic subunit of cAMP-dependent protein kinase. *J Biol Chem* **268**, 18626-18632 (1993).
57. Cauthron RD, Carter KB, Liauw S, Steinberg RA. Physiological phosphorylation of protein kinase A at Thr-197 is by a protein kinase A kinase. *Mol Cell Biol* **18**, 1416-1423 (1998).
58. Harraz OF, Welsh DG. Protein kinase A regulation of T-type Ca2+ channels in rat cerebral arterial smooth muscle. *J Cell Sci* **126**, 2944-2954 (2013).
59. Lory P, Nicole S, Monteil A. Neuronal Cav3 channelopathies: recent progress and perspectives. *Pflugers Arch* **472**, 831-844 (2020).
60. Kornhauser JM, Nelson DE, Mayo KE, Takahashi JS. Photic and circadian regulation of c-fos gene expression in the hamster suprachiasmatic nucleus. *Neuron* **5**, 127-134 (1990).

61. Honma S, *et al.* Dec1 and Dec2 are regulators of the mammalian molecular clock. *Nature* **419**, 841-844 (2002).
62. Golombek DA, Rosenstein RE. Physiology of circadian entrainment. *Physiol Rev* **90**, 1063-1102 (2010).
63. Olejniczak I, *et al.* Light affects behavioral despair involving the clock gene Period 1. *PLoS Genet* **17**, e1009625 (2021).
64. von Gall C, Noton E, Lee C, Weaver DR. Light does not degrade the constitutively expressed BMAL1 protein in the mouse suprachiasmatic nucleus. *Eur J Neurosci* **18**, 125-133 (2003).
65. Li L, Carter J, Gao X, Whitehead J, Tourtellotte WG. The neuroplasticity-associated arc gene is a direct transcriptional target of early growth response (Egr) transcription factors. *Mol Cell Biol* **25**, 10286-10300 (2005).
66. Reed HE, Meyer-Spasche A, Cutler DJ, Coen CW, Piggins HD. Vasoactive intestinal polypeptide (VIP) phase-shifts the rat suprachiasmatic nucleus clock in vitro. *Eur J Neurosci* **13**, 839-843 (2001).
67. Jones JR, Simon T, Lones L, Herzog ED. SCN VIP Neurons Are Essential for Normal Light-Mediated Resetting of the Circadian System. *J Neurosci* **38**, 7986-7995 (2018).
68. Jagannath A, *et al.* The CRTC1-SIK1 pathway regulates entrainment of the circadian clock. *Cell* **154**, 1100-1111 (2013).
69. Matsuo M, *et al.* A light-induced small G-protein gem limits the circadian clock phase-shift magnitude by inhibiting voltage-dependent calcium channels. *Cell Rep* **39**, 110844 (2022).
70. Alessandro MS, Golombek DA, Chiesa JJ. Protein Kinases in the Photic Signaling of the Mammalian Circadian Clock. *Yale J Biol Med* **92**, 241-250 (2019).
71. Ashton A, Foster RG, Jagannath A. Photic Entrainment of the Circadian System. *Int J Mol Sci* **23**, (2022).
72. Chavan R, *et al.* Liver-derived ketone bodies are necessary for food anticipation. *Nat Commun* **7**, 10580 (2016).
73. Zheng B, *et al.* The mPer2 gene encodes a functional component of the mammalian circadian clock. *Nature* **400**, 169-173 (1999).
74. Tarricone C, Dhavan R, Peng J, Areces LB, Tsai LH, Musacchio A. Structure and regulation of the CDK5-p25(nck5a) complex. *Mol Cell* **8**, 657-669 (2001).
75. Roach BL, Ngo JM, Limso C, Oloja KB, Bhandari D. Identification and characterization of a novel phosphoregulatory site on cyclin-dependent kinase 5. *Biochem Biophys Res Commun* **504**, 753-758 (2018).
76. Oberegelsbacher C, Schneidler C, Voolstra O, Cerny A, Huber A. The Drosophila TRPL ion channel shares a Rab-dependent translocation pathway with rhodopsin. *Eur J Cell Biol* **90**, 620-630 (2011).
77. Katz B, Payne R, Minke B. TRP Channels in Vision. In: *Neurobiology of TRP Channels* (ed Emir TLR) (2017).
78. Brancaccio M, Maywood ES, Chesham JE, Loudon AS, Hastings MH. A Gq-Ca2+ axis controls circuit-level encoding of circadian time in the suprachiasmatic nucleus. *Neuron* **78**, 714-728 (2013).
79. Zhang Y, *et al.* Fast and sensitive GCaMP calcium indicators for imaging neural populations. *Nature* **615**, 884-891 (2023).
80. Ding JM, *et al.* A neuronal ryanodine receptor mediates light-induced phase delays of the circadian clock. *Nature* **394**, 381-384 (1998).
81. Bibb JA, *et al.* Phosphorylation of DARPP-32 by Cdk5 modulates dopamine signalling in neurons. *Nature* **402**, 669-671 (1999).

82. Rossner MJ, *et al.* Disturbed clockwork resetting in Sharp-1 and Sharp-2 single and double mutant mice. *PLoS One* **3**, e2762 (2008).
83. Honrado GI, Johnson RS, Golombek DA, Spiegelman BM, Papaioannou VE, Ralph MR. The circadian system of c-fos deficient mice. *J Comp Physiol A* **178**, 563-570 (1996).
84. Riedel CS, Georg B, Jorgensen HL, Hannibal J, Fahrenkrug J. Mice Lacking EGR1 Have Impaired Clock Gene (BMAL1) Oscillation, Locomotor Activity, and Body Temperature. *J Mol Neurosci* **64**, 9-19 (2018).
85. Jud C, Schmutz I, Hampp G, Oster H, Albrecht U. A guideline for analyzing circadian wheel-running behavior in rodents under different lighting conditions. *Biol Proced Online* **7**, 101-116 (2005).

Acknowledgments

Technical assistance by Antoinette Hayoz and Maude Marmy is acknowledged. This work was supported by the Swiss National Science Foundation (SNF) 310030_219880/1 to UA, 310030_197607 to DAG, 310030_219438/1 to ZY, the Inselspital University Hospital Bern, the European Research Council CoG-725850 to AA and the States of Berne and Fribourg.

Author contributions

Conceived and designed the experiments: AB, UA.
Performed the experiments: AB, MB, GS, JR.
Analyzed the data: AB, MB, GS, JR, DG, AA, UA.
Contributed reagents, materials, analysis tools: DG, ZY, AA, UA
Wrote the paper: AB, UA

Competing interests

We declare no conflict of interest.

Figure legends:

Figure 1 Knock-down of Cdk5 in the SCN shortens period and reduces phase delays but not phase advances. (**a**) Examples of double plotted wheel-running actograms of control (scr) and Cdk5 knock-down (shCdk5) mice. Animals were kept under a 12 h light / 12 h dark cycle (white and grey areas, respectively) (LD). After 8-10 days they received a 15 min. light pulse at the indicated zeitgeber times (ZT) (yellow stars). After the light pulse animals were released into constant darkness (DD). This light pulse assessment is termed Aschoff type II. (**b**) Circadian period (τ) of shCdk5 mice (red) is significantly shorter compared to scr controls (blue). τ scr = 23.21 ± 0.08 h, τ shCdk5 = 22.47 ± 0.09 h. All values are mean ± SEM, unpaired t-test with Welch's correction, n = 6, ***p < 0.001. (**c**) Quantification of phase shifts (φ) after a 15 min. light pulse at ZT10, ZT14 and ZT22. The phase shift at ZT14 is strongly reduced in shCdk5 animals (red) compared to scr controls (blue). scr: φ ZT10: -1.93 ± 1.43 min., φ ZT14: -105.24 ± 1.54 min., φ ZT22: 34.30 ± 2.97 min., shCdk5: φ ZT10: -2.60 ± 1.72 min., φ ZT14: -11.80 ± 2.81 min., φ ZT22: 35.88 ± 5.68 min. All values are mean ± SEM, unpaired t-test with Welch's correction, n = 5-6, ****p < 0.0001. (**d**) Examples of double plotted wheel-running actograms of control (scr) and Cdk5 knock-down (shCdk5) mice. Animals were kept under DD. After 8-10 days they received a 15 min light pulse at the indicated circadian times (CT) (orange stars). This light pulse assessment is termed Aschoff type I. (**e**) Circadian period of shCdk5 mice (red) is significantly shorter compared to scr controls (blue). τ scr = 23.20 ± 0.05 h, τ shCdk5 = 22.48 ± 0.09 h. All values are mean ± SEM, unpaired t-test with Welch's correction, n = 5, ***p < 0.001. (**f**) Quantification of phase shifts after a 15 min. light pulse at CT10, CT14 and CT22. The phase shift at CT14 is strongly reduced in shCdk5 animals (red) compared to scr controls (blue). scr: φ ZT10: 0.12 ± 3.31 min., φ ZT14: -121.52 ± 8.18 min., φ ZT22: 48.40 ± 3.43 min., shCdk5: φ ZT10: -1.68 ± 2.78 min., φ ZT14: -46.60 ± 5.84 min., φ ZT22: 54.16 ± 3.19 min. All values are mean ± SEM, unpaired t-test with Welch's correction, n = 5, ***p < 0.001.

Figure 2 Cdk5 activity is modulated by light in the early night. Immuno Western blotting (IB), immunoprecipitation (IP) and Cdk5 kinase activity assays from SCN tissue extracts harvested 30 min after light (+) and no light (-) given at ZT14. (**a**) Western blot depicting the amounts of phospho PKA (p-PKA), p35 co-activator, Cdk5 and tubulin (Tub, control) before and after light pulse at ZT14. (**b**) Quantification of p-PKA relative to tubulin. Values are the mean ± SEM. Unpaired t-test, n = 3, *p < 0.05. (**c**) Quantification of p35 co-activator of Cdk5. Values are the mean ± SEM. Unpaired t-test, n = 3, ***p < 0.001. (**d**) Cdk5 kinase activity assay. IP of SCN extract with antibodies against Cdk5 showing presence of Cdk5 (upper panel) and total protein with Coomassie blue staining (lower panel) as control for the presence of H1. The middle panel depicts histone H1 phosphorylated by Cdk5, visualized as ^{32}P-histone H1 (^{32}P-H1). (**e**) Quantification of Cdk5 kinase activity relative to H1 levels. Values are the mean ± SEM. Unpaired t-test, n = 3, ***p < 0.001. (**f**) Co-immunoprecipitation of p35 with Cdk5 before and after a light pulse.

Figure 3 Cdk5 impacts on the CREB signaling pathway via calcium/calmodulin dependent kinases (CaMK). The cartoons on the left of each figure depict the CaMK pathway with the red rectangle indicating the visualization of a particular the component. (**a**) Immunohistochemistry on the SCN of control (scr) and shCdk5 mice using an antibody recognizing phospho-serine 133 of CREB (p-CREB-S133) before and after a light pulse at ZT14. The red color shows p-CREB-S133 and the blue color represents Dapi stained nuclei of SCN cells. Scale bar: 8 µm. The right panel shows the quantification of p-CREB-S133 signal. Values are the mean ± SEM. Unpaired t-test with Welch's correction, n = 3, *p < 0.05.

(**b**) Immunohistochemistry on the SCN of control (scr) and shCdk5 mice using an antibody recognizing Cam kinase II (CaMKII) before and after a light pulse at ZT14. The red color shows CaMKII and the blue color represents Dapi stained nuclei of SCN cells. Scale bar: 8 µm. The right panel shows the quantification of CaMKII signal. Values are the mean ± SEM. Unpaired t-test with Welch's correction, n = 3, *p < 0.05. (**c**) Translocation of calmodulin (CAM) in response to a light pulse at ZT14 in SCN neurons of control (scr) and Cdk5 knock-down (shCdk5) animals. CAM (yellow) accumulates around the nuclei in scr controls. In shCdk5 SCN neurons this accumulation around the nuclei is already seen before the light pulse which is clearly different from scr controls. Scale bar: 7 µm The right panel shows the quantification of CAM rings. Values are the mean ± SEM. Unpaired t-test with Welch's correction, n = 3, *p < 0.05, **p < 0.01. (**d**) Immunohistochemistry on the SCN of control (scr) and shCdk5 mice using an antibody recognizing Cam kinase IV (CaMKIV) before and after a light pulse at ZT14. The red color shows CaMKIV and the blue color represents Dapi stained nuclei of SCN cells. Scale bar: 5 µm. The right panel shows the quantification of CaMKIV signal. Values are the mean ± SEM. Unpaired t-test with Welch's correction, n = 3, *p < 0.05. (**e**) Immunohistochemistry on the SCN of control (scr) and shCdk5 mice using an antibody recognizing the calcium channel Cav3.1 before and after a light pulse at ZT14. The green color shows Cav3.1 and the blue color represents Dapi stained nuclei of SCN cells. Scale bar: 5 µm. The right panel shows the relative Cav3.1 signal. Values are the mean ± SEM. Unpaired t-test with Welch's correction, n = 3, *p < 0.05.

Figure 4 Neuronal activity in response to light at ZT14 is modulated by CDK5. (**a**) Illustration of the chronic optic fiber implantation in the SCN for fiber photometry recording in freely moving mice (left). The animals were previously infected either with AAV9-hSyn1-chl[1x(shNS)]-jGCaMP7b-WPRE-SV40p(A)(scr) or AAV9-hSyn1-chl[mouse(shCdk5)]-jGCaMP7b-WPRE-SV40p(A)(shCdk5). The experimental timeline of one trial is shown on the right. White and dark boxes represent light and dark phase, respectively. Fiber photometry experiments were performed in the 5 min. before and 15 min. after the 15 min. light pulse delivered at ZT14 (blue box; dashed lines between minutes 14-15 are not included in the analysis). (**b**) Representative traces of cell activity (normalized $\Delta F/F_0$) of GCaMP7b-expressing SCN neurons (black: scr, red: shCdk5) in the dark phase, 5 min. before and 15 min. after the 15 min. (± 20 s) light pulse delivered at ZT14. (**c**) Bar plot showing the percentage of $\Delta F/F_0$ changes ± SEM 5 min. before the light pulse, in the first and last 5 min. during the light pulse and the first and last 5 min. after the light pulse. *9-14 minutes of light pulse*: scramble (black bar) 105.5 ± 19.3 $\Delta F/F_0$ vs. shCdk5 (red bar) 74.7 ± 17.2 $\Delta F/F_0$. *1-5 minutes after light pulse*: scramble (black bar) 111.2 ± 19.3 $\Delta F/F_0$ vs. shCdk5 (red bar) 81.0 ± 17.8 $\Delta F/F_0$. Black = scr, N = 15 trials, n = 5 mice / red = shCdk5, N = 12 trials, n = 4 mice. Bar values represent the mean ± SEM. ***p < 0.001; two-way ANOVA corrected with Bonferroni post-hoc test. (**d**) Photomicrograph of the expression of GCaMP7b (green) in the SCN in both control (scr, left) and experimental (shCdk5, right) animals. The red hatched oval indicates the placement of the optic fiber. Blue: Dapi, green: GFP (produced by jGCaMPP7). Scale bar 50 µm.

Figure 5 CDK5 regulates PKA phosphorylation via DARPP32 phosphorylation. (**a**) Top: Scheme of the forskolin-PKA-CREB signaling pathway. Bottom: FRET/CFP signal ratio changes in response to forskolin treatment in NIH 3T3 cells transfected with either a scr control (blue) or shCdk5 (red) expression construct. Values are the mean ± SD. Two-way ANOVA revealed a significant difference between the curves, n = 3, ****p < 0.0001. (**b**) Top: Scheme of the forskolin-PKA-CREB signaling pathway and calcium signaling. Bottom: FRET/CFP signal ratio changes in response to forskolin treatment in NIH 3T3 cells with

addition of Ca^{2+} (blue), without addition of Ca^{2+} (salmon colored) and with addition of Ca^{2+} and EGTA (orange). Values are the mean ± SD. Two-way ANOVA revealed a significant difference between the grey and blue/orange curves, n = 3, ****p < 0.0001. (**c**) Scheme of CDK5-DARPP32-PKA pathway. (**d**) Immunohistochemistry on the SCN of control (scr) and shCdk5 mice using an antibody recognizing phosphorylated Thr-75 of DARPP32 (p-DARPP32) before and after a light pulse at ZT14. The red color shows p-DARPP32 and the blue color represents Dapi stained nuclei of SCN cells. Scale bar: 10 µm. The right panel shows the quantification of p-DARPP32 signal. Values are the mean ± SEM. Unpaired t-test with Welch's correction, n = 3, **p < 0.01. (**e**) Immunohistochemistry on the SCN of control (scr) and shCdk5 mice using an antibody recognizing phosphorylated Thr-197 of PKA (p-PKA) before and after a light pulse at ZT14. The red color shows p-PKA and the blue color represents Dapi stained nuclei of SCN cells. Scale bar: 20 µm. The right panel shows the quantification of p-PKA signal. Values are the mean ± SEM. Unpaired t-test with Welch's correction, n = 3, *p < 0.05, **p < 0.01. (**f**) Immunohistochemistry on the SCN of control (scr) and shCdk5 mice using an antibody recognizing phosphorylated Thr-197 of PKA (p-PKA) and Cav3.1 before and after a light pulse at ZT14. The red color shows p-PKA, the green color Cav3.1 and the blue color represents Dapi stained nuclei of SCN cells. The yellow color signifies co-localization of PKA and Cav3.1. The stripes on the left and bottom of each micrograph show the z-stacks to confirm co-localization. Scale bar: 10 µm. The right panel shows the quantification of relative p-PKA/Cav3.1. Values are the mean ± SEM. Unpaired t-test with Welch's correction, n = 3, *p < 0.05.

Figure 6 Cdk5 is regulating light induced gene expression in the SCN of some clock genes. Relative mRNA values are represented as blue bars for scr control animals and as red bars for shCdk5 mice. The values were determined 0, 0.5, 1 and 2 hours after a light pulse (LP) given at ZT14. (**a**) Induction of *Per1* mRNA expression by light with a maximum at 1 hour after light in scr control animals. In contrast *Per1* is not induced in shCdk5 SCN. Scr: 0 h: 0.44 ± 0.01, 0.5 h: 0.65 ± 0.12, 1 h: 1.12 ± 0.19, 2 h: 0.44 ± 0.01; shCdk5: 0 h: 0.44 ± 0.01, 0.5 h: 0.44 ± 0.01, 1 h: 0.44 ± 0.01, 2 h: 0.77 ± 0.18. Values are the mean ± SEM. Unpaired t-test, n = 3, *p < 0.05. (**b**) *Per2* mRNA expression is not induced by light neither in scr controls nor in shCdk5 animals. Scr: 0 h: 1.04 ± 0.16, 0.5 h: 0.95 ± 0.10, 1 h: 0.83 ± 0.10, 2 h: 0.96 ± 0.07; shCdk5: 0 h: 1.01 ± 0.05, 0.5 h: 1.07 ± 0.10, 1 h: 1.04 ± 0.14, 2 h: 1.04 ± 0.12. Values are the mean ± SEM. Unpaired t-test, n = 3 (**c**) Induction of *Dec1* mRNA expression by light with a maximum at 1 hour after light in scr control animals. In contrast *Dec1* is not induced in shCdk5 SCN. Scr: 0 h: 1.87 ± 0.37, 0.5 h: 3.32 ± 0.75, 1 h: 4.25 ± 0.49, 2 h: 3.13 ± 0.34; shCdk5: 0 h: 1.96 ± 0.34, 0.5 h: 2.13 ± 0.51, 1 h: 1.87 ± 0.07, 2 h: 2.32 ± 0.40. Values are the mean ± SEM. Unpaired t-test, n = 3, *p < 0.05. (**d**) *Dec2* mRNA expression is not induced by light neither in scr controls not in shCdk5 animals. Scr: 0 h: 1.93 ± 0.29, 0.5 h: 1.94 ± 0.25, 1 h: 1.75 ± 0.49, 2 h: 2.11 ± 0.07; shCdk5: 0 h: 1.94 ± 0.23, 0.5 h: 1.58 ± 0.07, 1 h: 1.61 ± 0.25, 2 h: 1.90 ± 0.33. Values are the mean ± SEM. Unpaired t-test, n = 3. (**e**) *Bmal1* mRNA expression is not induced by light in the SCN of scr control and shCdk5 animals. Scr: 0 h: 0.60 ± 0.04, 0.5 h: 0.69 ± 0.06, 1 h: 0.65 ± 0.05, 2 h: 0.81 ± 0.12; shCdk5: 0 h: 0.61 ± 0.14, 0.5 h: 0.61 ± 0.12, 1 h: 0.56 ± 0.06, 2 h: 0.71 ± 0.15. Values are the mean ± SEM. Unpaired t-test, n = 3. (**f**) *eGFP* mRNA expression is detected in the SCN of scr control and shCdk5 animals demonstrating proper injection of expression constructs (scr: ssAAV-9/2-hSyn1-chl[1x(shNS)]-EGFP-WPRE-SV40p(A), shCdk5: ssAAV-9/2-hSyn1-chl[mouse(shCdk5)]-EGFP-WPRE-SV40p(A)). Scr: 0 h: 1.04 ± 0.19, 0.5 h: 1.23 ± 0.22, 1 h: 0.90 ± 0.07, 2 h: 1.34 ± 0.34; shCdk5: 0 h: 1.31 ± 0.28, 0.5 h: 1.04 ± 0.13, 1 h: 0.90 ± 0.05, 2 h: 1.15 ± 0.06. Values are the mean ± SEM. Unpaired t-test, n = 3. (**g**) Induction of *cFos* mRNA 0.5 hours after the light pulse in both scr controls and shCdk5 SCN. Scr: 0 h: 0.77 ±

0.07, 0.5 h: 2.55 ± 0.38, 1 h: 0.64 ± 0.25, 2 h: 0.61 ± 0.15; shCdk5: 0 h: 0.95 ± 0.08, 0.5 h: 2.57 ± 0.05, 1 h: 0.68 ± 0.04, 2 h: 0.74 ± 0.12. Values are the mean ± SEM. Unpaired t-test, n = 3, *p < 0.05, ***p < 0.001. (**h**) Induction of *Egr1* mRNA 0.5 hours after the light pulse in scr control but not shCdk5 SCN. Scr: 0 h: 1.25 ± 0.38, 0.5 h: 2.71 ± 0.19, 1 h: 2.12 ± 0.41, 2 h: 1.26 ± 0.13; shCdk5: 0 h: 1.23 ± 0.24, 0.5 h: 1.77 ± 0.13, 1 h: 1.16 ± 0.08, 2 h: 1.18 ± 0.06. Values are the mean ± SEM. Unpaired t-test, n = 3, *p < 0.05. (**i**) *Sik1* mRNA expression is induced by light in the SCN of scr control but not shCdk5 animals. Scr: 0 h: 0.29 ± 0.07, 0.5 h: 0.58 ± 0.02, 1 h: 0.27 ± 0.14, 2 h: 0.34 ± 0.07; shCdk5: 0 h: 0.22 ± 0.03, 0.5 h: 0.20 ± 0.01, 1 h: 0.19 ± 0.02, 2 h: 0.25 ± 0.02. Values are the mean ± SEM. Unpaired t-test, n = 3, *p < 0.05, **p < 0.01. (**j**) *Gem* mRNA expression is induced by light in the SCN of scr control but not shCdk5 animals. Scr: 0 h: 0.70 ± 0.07, 0.5 h: 0.86 ± 0.05, 1 h: 1.38 ± 0.11, 2 h: 0.94 ± 0.11; shCdk5: 0 h: 1.05 ± 0.24, 0.5 h: 1.08 ± 0.03, 1 h: 1.13 ± 0.07, 2 h: 0.93 ± 0.05. Values are the mean ± SEM. Unpaired t-test, n = 3, *p < 0.05.

Figure 7 Model of Cdk5 gated light signal. (**a**) Cdk5 is active during the dark portion of the day. Active Cdk5 with its co-activator p35 phosphorylates PER2, which leads to stabilization and nuclear translocation of this protein that is abundant at ZT12. At the same time CDK5 phosphorylates DARPP32, which inhibits the PKA signaling pathway. (**b**) Light perceived in the dark phase at ZT14 leads to detachment of p35 from Cdk5 stopping Cdk5 activity. DARPP32 is not phosphorylated and hence can't inhibit PKA. PKA that is activated by the light signal is phosphorylated and can mediate CREB phosphorylation via T-type calcium channels (Cav3.1) and the CaMK pathway leading to a transcriptionally active complex on the CRE element present in the promoters of many light responsive genes such as *Per1*, *Dec1*, *Gem* and *Sik1*. Overall, a light pulse at ZT14 will activate CREB phosphorylation and a protein complex will form. This complex needs phosphorylated PER2 that has accumulated in the nucleus between ZT12 and ZT14 to initiate transcription of light responsive genes. Both arms are necessary to build up a transcriptionally functional complex. Both arms depend on the presence and activity of CDK5, which therefore gates the light signal at ZT14. It is very likely that the amount of PER2 protein in the nucleus determines at least in part the magnitude of the phase delay, which depends on the timing of the light signal.

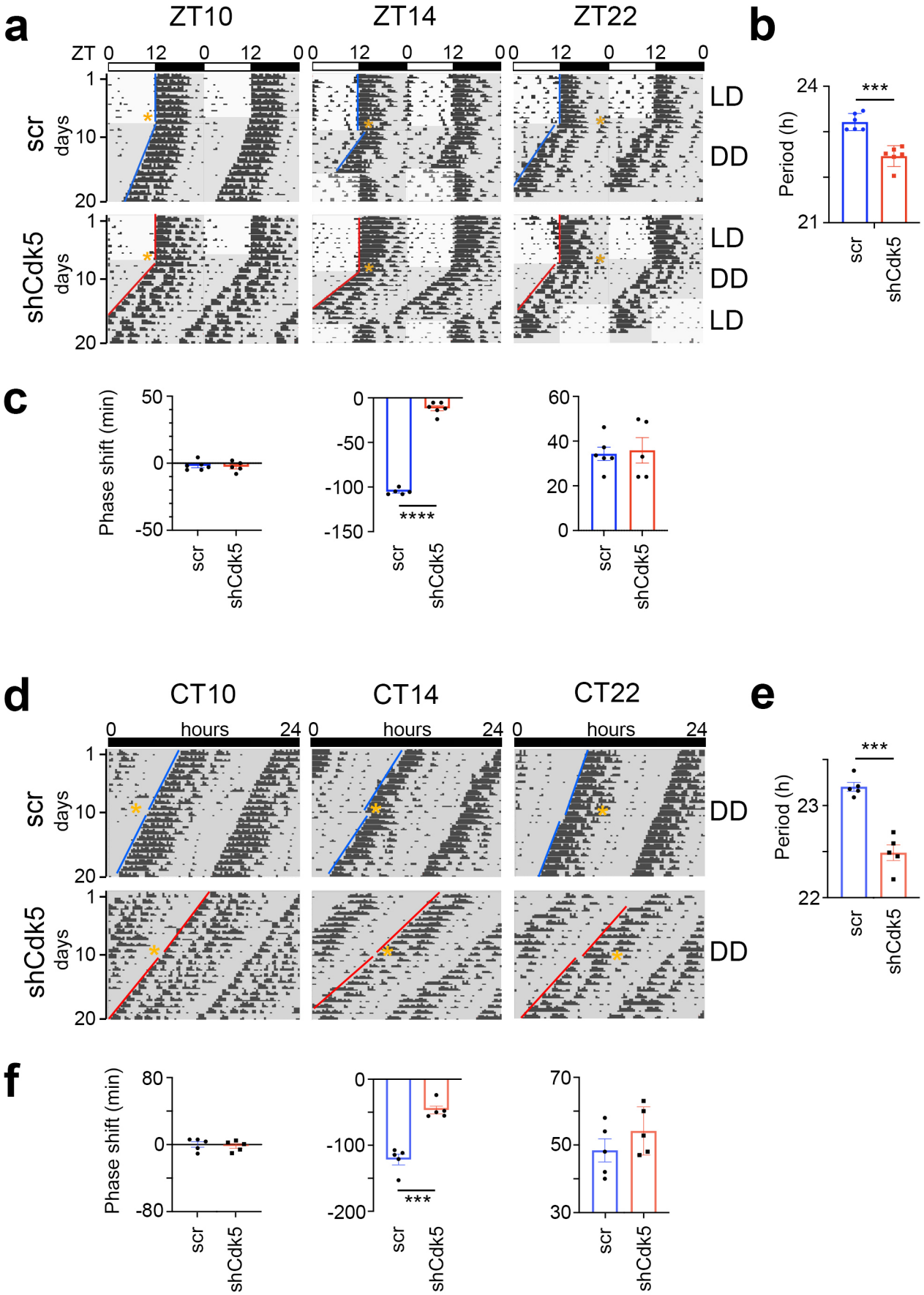
a
ZT10
ZT14
ZT22
ZT 0 12 0 12 0
scr
shCdk5
days
1
10
20
LD
DD
b
Period (h)
24
21
***
scr
shCdk5
c
Phase shift (min)
50
0
-50
-100
-150
****
60
40
20
d
CT10
CT14
CT22
0 hours 24
DD
e
Period (h)
23
22
***
f
Phase shift (min)
80
-80
-200
70
50
30

Fig. 1

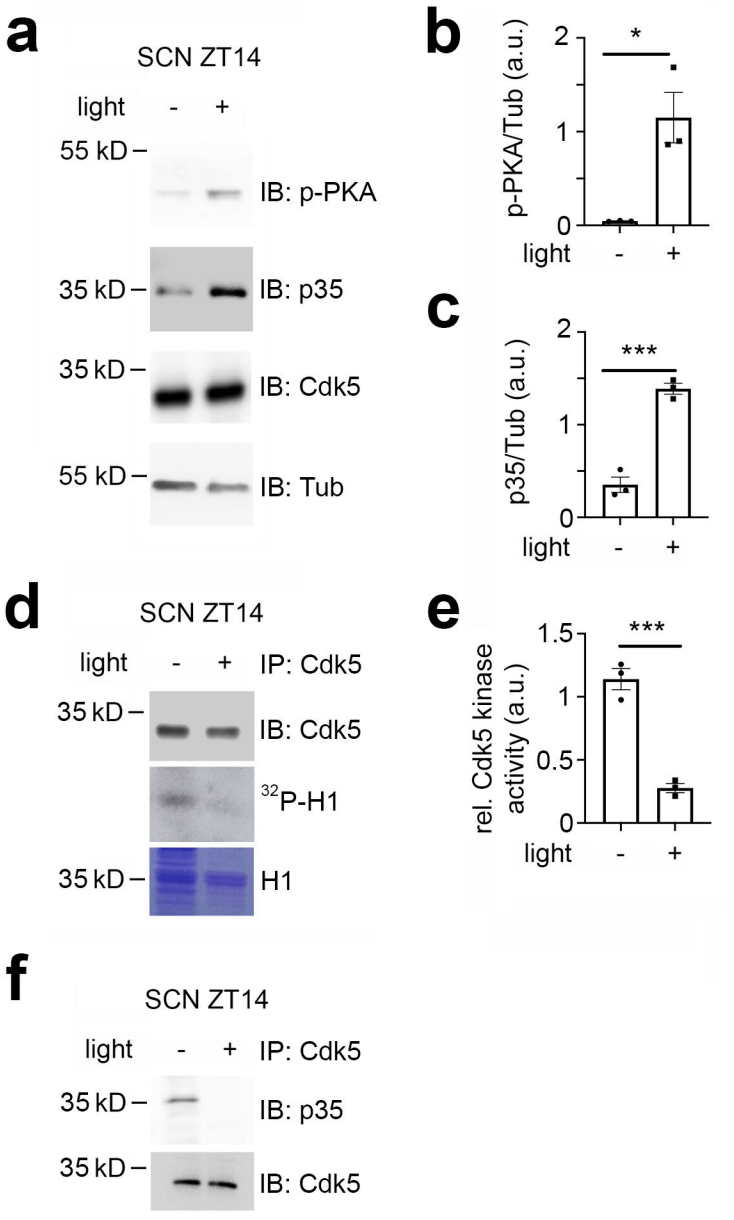
a
SCN ZT14
light - +
55 kD
IB: p-PKA
35 kD
IB: p35
35 kD
IB: Cdk5
55 kD
IB: Tub
b
p-PKA/Tub (a.u.)
2
1
0
*
light - +
c
p35/Tub (a.u.)
2
1
0
***
light - +
d
SCN ZT14
light - + IP: Cdk5
35 kD
IB: Cdk5
32P-H1
35 kD
H1
e
rel. Cdk5 kinase activity (a.u.)
1.5
1
0.5
0
***
light - +
f
SCN ZT14
light - + IP: Cdk5
35 kD
IB: p35
35 kD
IB: Cdk5

Fig. 2

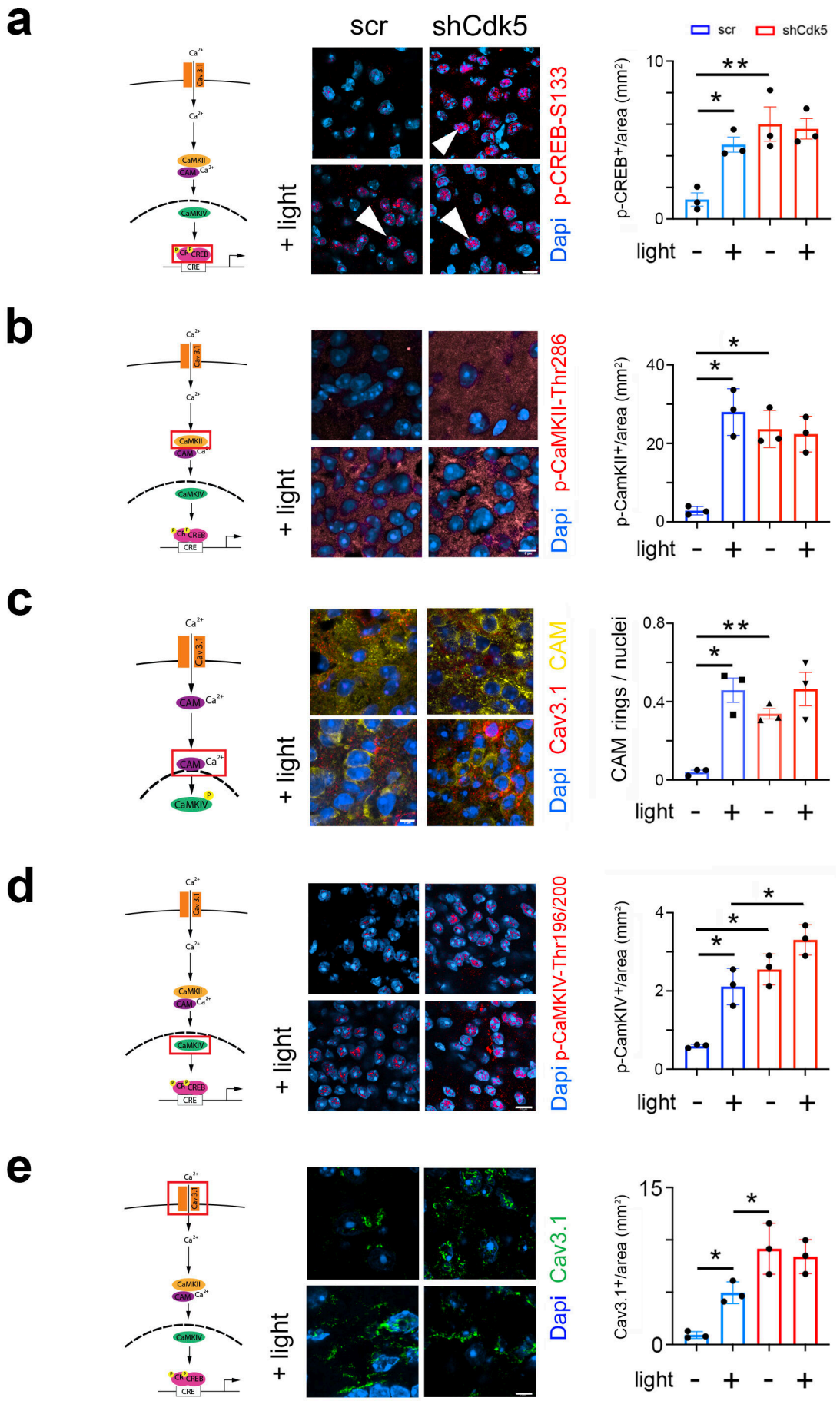
a
scr
shCdk5
scr
shCdk5
+ light
Dapi p-CREB-S133
p-CREB+/area (mm2)
10
0
light - + - +
b
+ light
Dapi p-CaMKII-Thr286
p-CamKII+/area (mm2)
40
20
0
light - + - +
c
+ light
Dapi Cav3.1 CAM
CAM rings / nuclei
0.8
0.4
0
light - + - +
d
+ light
Dapi p-CaMKIV-Thr196/200
p-CamKIV+/area (mm2)
4
2
0
light - + - +
e
+ light
Dapi Cav3.1
Cav3.1+/area (mm2)
15
0
light - + - +

Fig. 3

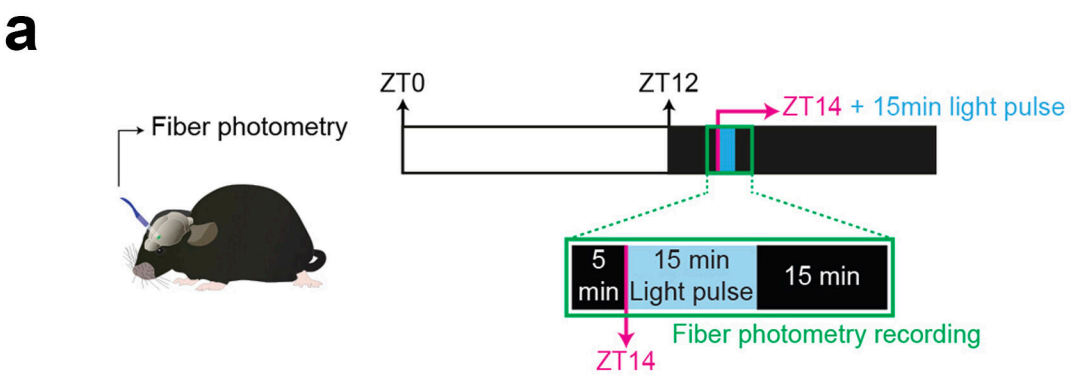
a
ZT0
ZT12
ZT14 + 15min light pulse
Fiber photometry
5 min
15 min Light pulse
15 min
Fiber photometry recording
ZT14

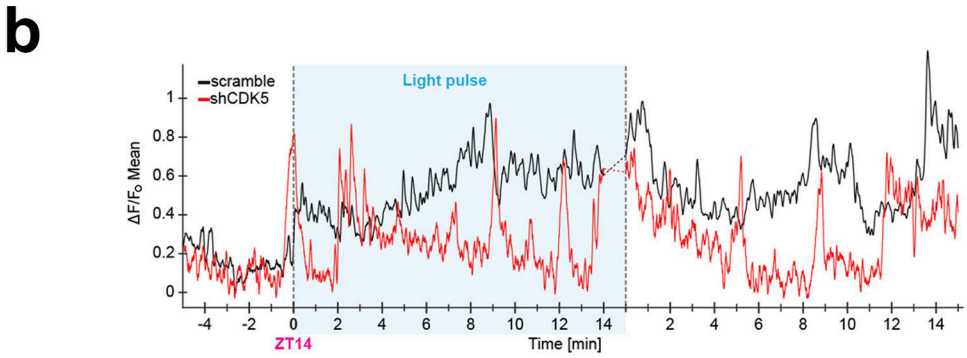
b
scramble
shCDK5
Light pulse
ΔF/F0 Mean
ZT14
Time [min]

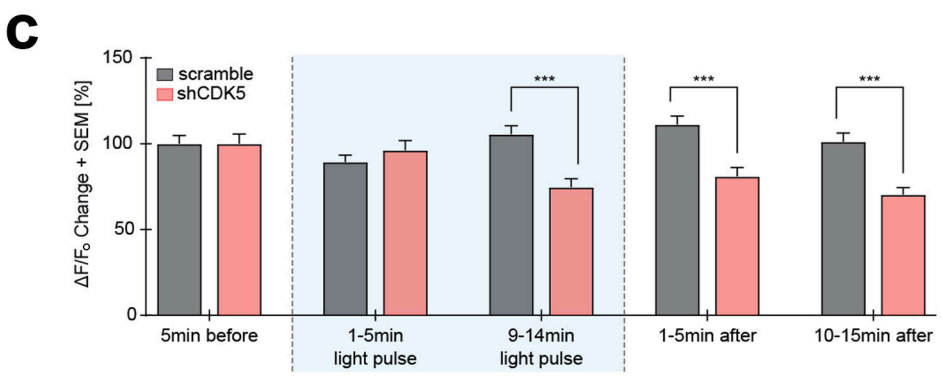
c
scramble
shCDK5
ΔF/F0 Change + SEM [%]
***
5min before
1-5min light pulse
9-14min light pulse
1-5min after
10-15min after

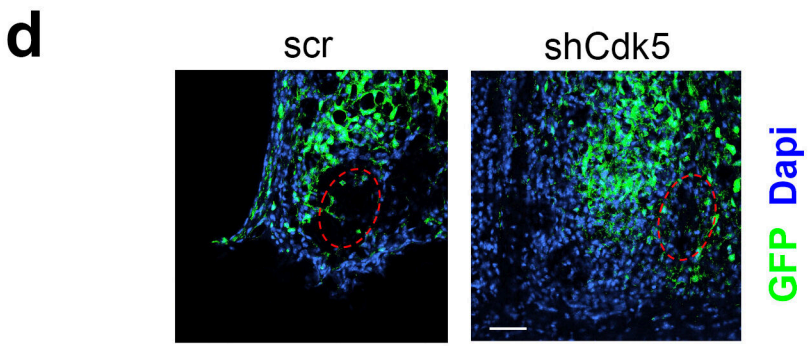
d
scr
shCdk5
GFP Dapi

Fig. 4

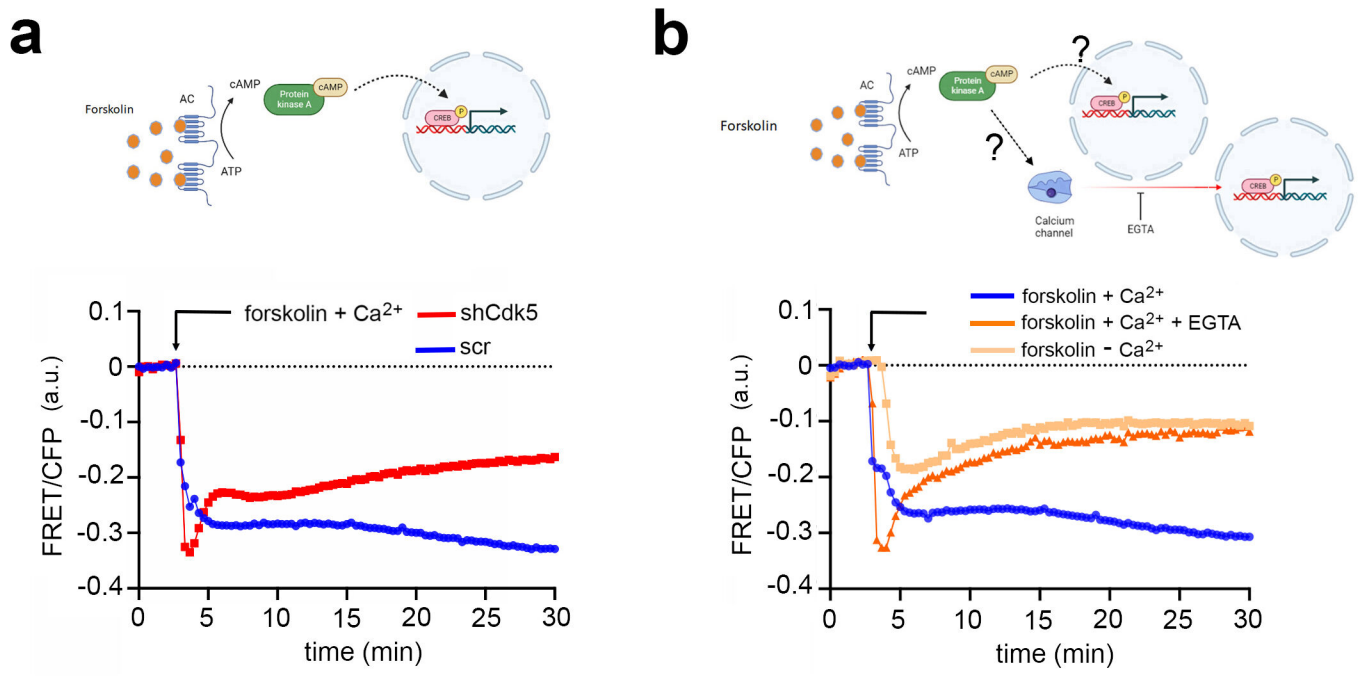

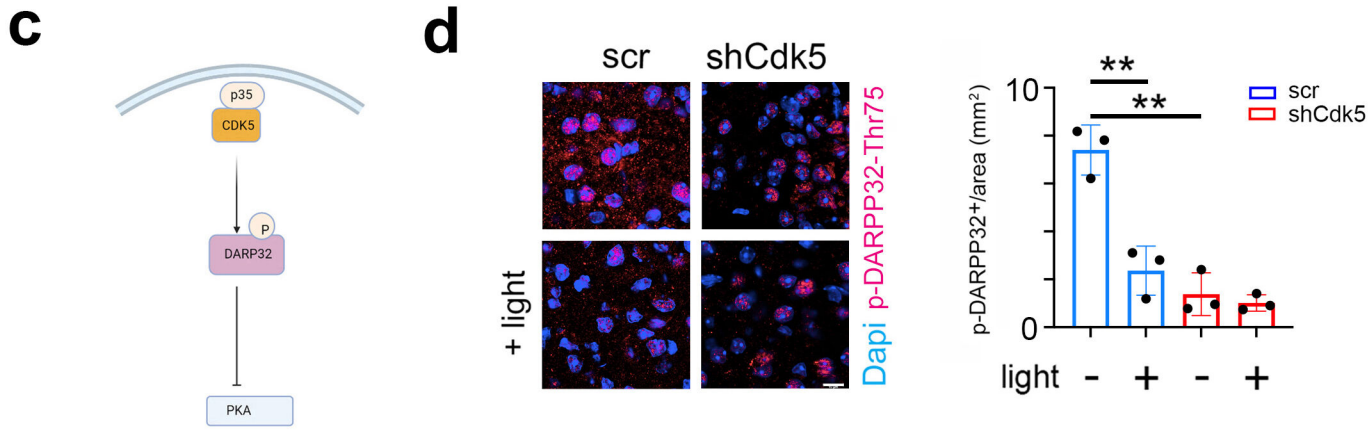

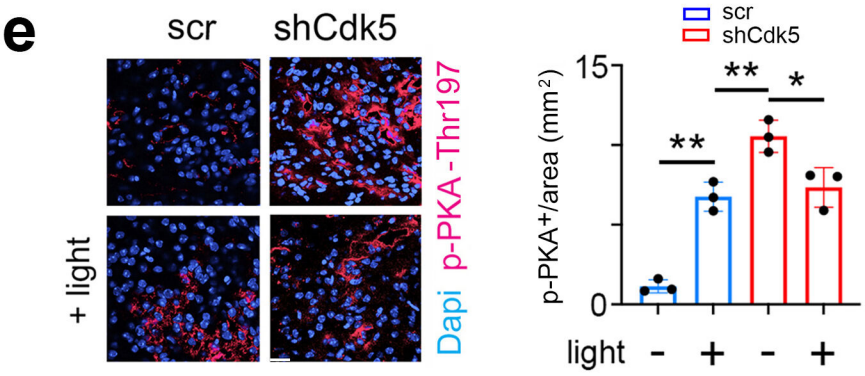

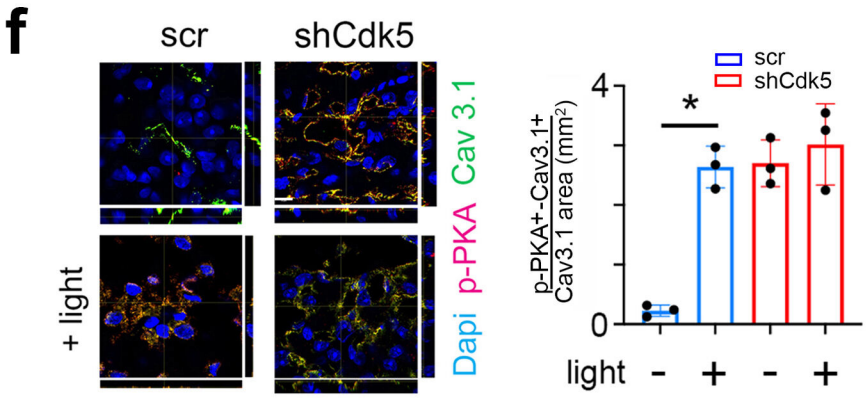

Fig. 5

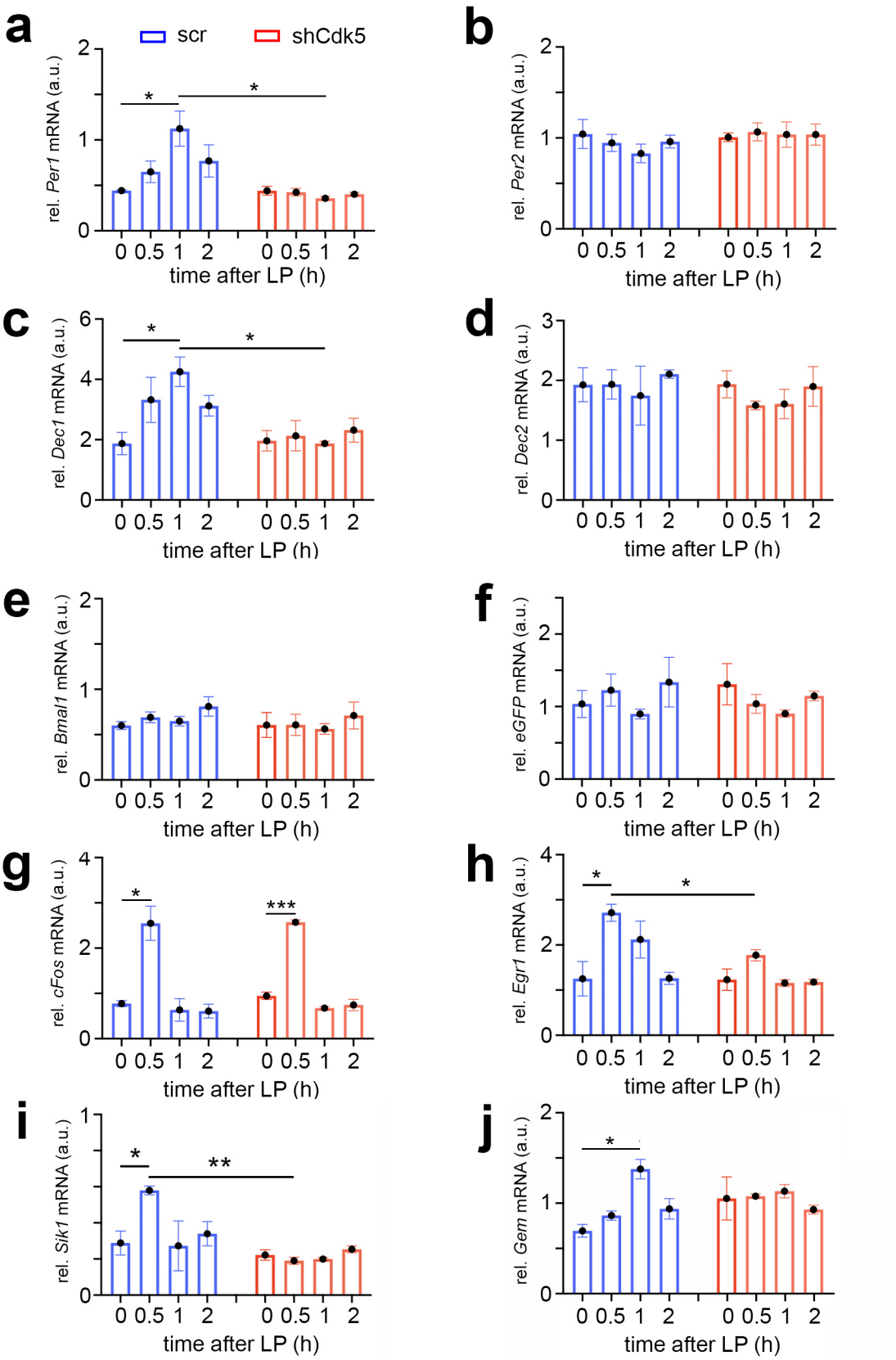
a
scr
shCdk5
rel. Per1 mRNA (a.u.)
b
rel. Per2 mRNA (a.u.)
c
rel. Dec1 mRNA (a.u.)
d
rel. Dec2 mRNA (a.u.)
e
rel. Bmal1 mRNA (a.u.)
f
rel. eGFP mRNA (a.u.)
g
rel. cFos mRNA (a.u.)
h
rel. Egr1 mRNA (a.u.)
i
rel. Sik1 mRNA (a.u.)
j
rel. Gem mRNA (a.u.)
0 0.5 1 2 0 0.5 1 2
time after LP (h)

Fig. 6

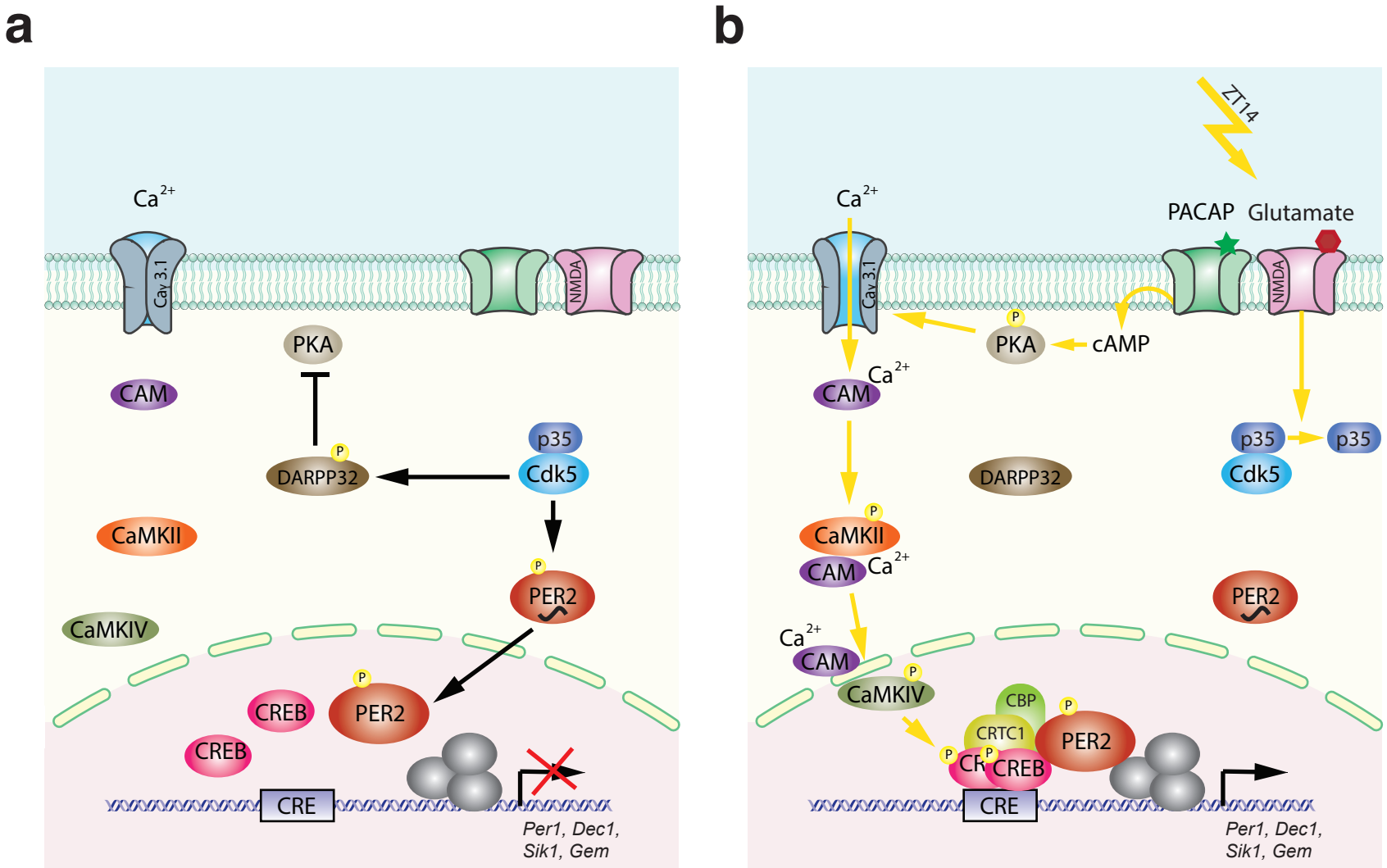
a
b
Ca2+
Cav 3.1
NMDA
PKA
CAM
DARPP32
p35
Cdk5
CaMKII
PER2
CaMKIV
CREB
CRE
Per1, Dec1,
Sik1, Gem
ZT14
PACAP
Glutamate
cAMP
CBP
CRTC1

Fig. 7